

© 2018 by Long Zhou. All rights reserved.

EMBEDDABLE MICRO PINCH VALVE FOR LOCALIZED PRESSURE CONTROL ON
MODULAR PNEUMATIC SOFT ROBOTIC ARM

BY
LONG ZHOU

THESIS

Submitted in partial fulfillment of the requirements
for the degree of Master of Science in Nuclear, Plasma, and Radiological Engineering
in the Graduate College of the
University of Illinois at Urbana-Champaign, 2018

Urbana, Illinois

Master's Committee:

Associate Professor Yang Zhang, Chair
Assistant Professor Angela Di Fulvio

Abstract

The advantages of soft robots include being able to manipulate delicate objects, adaptive to uncertain and dynamic task-environments and interacting with human in an intrinsically friendly manner. These merits make them potentially useful in the nuclear industry, where robots have to handle different situations involving radiation. Despite numerous designs for actuators, most soft robots nowadays are still driven by external valves and energy supplies. This gives rise to the problem that every actuator on the robot has to be connected by a tube to the outside, which hinders the agility and limits the scalability of the robot. Localizing the fluid control can reduce the number of tubes connecting to soft robots, especially for those with many degrees of freedom (DoFs). It also enables modular design, which allows the robots to be reconfigured for different tasks. To achieve localized control with minimal additional weight and size, we designed the embeddable micro pinch valve (EMPV) that is light ($< 2.5\text{ g}$) and small ($< 2\text{ cm}^3$) enough to be built into a typical soft pneumatic actuator. An EMPV manipulates the flow going into (or out from) the actuator by externally squeezing the channel that connects the actuator to the pressure source. This reduces the need of sealing components because the integrity of the flow channels is preserved. Combining two EMPVs and a soft pneumatic actuator, we designed a hybrid actuator that is controlled by electric signals while powered by pneumatic force. Then, a prototype wrist module with three degrees of freedom is made using three hybrid actuators. A circuit locally controls the EMPVs on the wrist and communicates with the central controller via Isomorphic Synchronous Transmit-Receive (ISTR) protocol which is specially designed for modular robots. Connecting several identical copies of the wrist in series, we built up a modular soft robotic arm. These prototypes aim to demonstrate that, with EMPVs, all the actuators on a pneumatic soft robot can be powered by a set of arterial pressure supplies, thus more actuators can be built into a soft robot without adding cumbersome tubes, making the soft robot more dexterous and biomimetic.

Acknowledgments

This project would not have been possible without the support of my PI, Prof Yang Zhang. It is the time and effort he spent in developing this emerging area ensures the swift progress of all the work. He also encourages me to explore bravely in the field and invest for the instruments I need. I really enjoy the culture of the group.

I would like to thank two undergraduate students, Riley Dylan Camp and Zhongyi Shen, who helped me preparing some of the parts used in the prototype.

Special thanks to another graduate student, Xinghua Liu, who helped me testing the circuit design and wrote part of the code for ISTR protocol. Furthermore, he also provided many useful ideas on the trend and the future of the field in our discussions.

Finally, I must express my very profound gratitude to my wife, who always supports my decision and works hard for our future. All these years we struggle together and dream together, with the faith that our fate is in our own hands.

Table of Contents

List of Figures	v
List of Abbreviations	vii
Chapter 1 Introduction	1
1.1 Soft Robot	1
1.2 Soft Actuators	2
1.3 Fluid-driven Soft Robot	5
1.4 Modular Soft Robot	6
Chapter 2 Embeddable Fluid Controller	8
2.1 Embeddable Micro Pinch Valve	8
2.2 Fabrication of the EMPV	10
2.3 Squeezing Mechanism	11
2.3.1 Squeezing Force Measurement	12
2.4 Response Time of EMPV	13
2.4.1 Response Time Measurement	16
Chapter 3 Hybrid Actuator	18
3.1 Local Three-state Controller	18
3.2 Prototype Hybrid Actuator	19
3.2.1 3D-printed LTC Frame	20
3.2.2 Miniature Tube-to-channel Fitting	21
3.2.3 Fabrication of the Silicone Pneumatic Spring	22
3.2.4 Soft Actuator Fitting	23
3.2.5 Driver Circuit	25
3.3 Feedback Control Demo	25
Chapter 4 Modular Soft Robotic Arm	28
4.1 Modular Design	28
4.1.1 Control Circuit	30
4.1.2 Prototype Wrist	31
4.2 Modular Soft Arm	32
4.3 Isomorphic Synchronous Transmit-Receive	34
Chapter 5 Discussion	38
References	40

List of Figures

1.1	PneuNets Bending Actuator by Whitesides Research Group, pictures taken from Ref[12]	2
1.2	Fiber-Reinforced Actuators, pictures taken from softroboticstoolkit.com	3
1.3	(A) DEA, pictures taken from Ref[17] and (B) IPMC, pictures taken from Ref[18]	4
1.4	Soft robots made in labs. (A) A tethered soft robot worm by WPI Soft Robotics Lab; (B) HPN Manipulator by Jiang et al., picture taken from Ref[25]; (C) 2D-soft arm by Robert et al, picture taken from Ref[26]; (D) 1-DoF robotics fish by Andrew et al, picture taken from Ref[27]. Except robots with less DoFs (e.g. (D)), most fluid-driven soft robot are tethered by tubes.	5
1.5	Modular soft robot designed by Roberton et al., picture taken from Ref[32]	7
2.1	Basic structure and two states (open and closed) of the valve, close is the normal state.	8
2.2	The dimensions of the EPV assembly.	9
2.3	Schematic diagram of the working principle of the EMPV. The permanent magnet attracts the steel plunger in closed state. A reverse magnetic field generated by the energized solenoid can cancel the attraction and release the plunger, which allows the tube to recovery to its original shape by both pressure and elasticity.	10
2.4	Closing force for different inlet pressure, relative to ambient.	11
2.5	Experiment set up to measure the squeezing force	12
2.6	Response time for different inlet pressure	13
2.7	Typical response curve of energizing an EMPV	14
2.8	Detailed energizing process. The average opening time of the EMPV is 7ms.	15
2.9	Typical response curve of closing an EMPV by reverse current.	15
2.10	The details of closing process	16
2.11	Response time measurement setup	17
3.1	The working principle of three-state controller. Noting only when the actuator is changing its length does it consume current.	19
3.2	A rendered hybrid actuator. Two EMPVs are used to control the pressurizing and exhausting of the actuator. A dual H-bridge driver controls the polarity of the voltage applied to each EMPV according to the input.	20
3.3	Actual LTC before mounting the local control circuit. The built-in flow channels can be seen in the middle of the frame.	21
3.4	Miniature tube-to-channel fitting	22
3.5	The molds used for silicone injection	22
3.6	The molds used for the inner wax mold	23
3.7	Fitting for soft pneumatic actuator	24
3.8	Connection to the hybrid actuator	24
3.9	Driver circuit of the hybrid actuator. (A) Circuit schematic (B) Board layout	25
3.10	Feedback control demonstration, noting in all (A) to (C) the actuator is in hold state (No energy consumption).	26
3.11	Connections and experiment setup.	27

4.1	A 3-DoF modular wrist made of three hybrid actuators with low-profile TLCs (rendered).	28
4.2	Instead of placing the EPVs along the actuator axis, low-profile LTC have both EPVs on the side, providing better thermal dissipation and consuming less space along the actuator. (1) Actuator fitting, (2) EPV, (3) circuit board, (4) programming pins, (5) communication header, (6) printed flow channel, (7) Printed three-way dual-channel pressure distributor, (8) Dual-channel pressure supply connector, (9) Arterial supply tubes in double helix shape, (10) Actuator, (11) Connector to previous section (12) connector to next module. (13) pressure connector to next module. (14) Vertebra plates confine the deformation of the actuators.	29
4.3	Schematic structure of the control circuit, EPVs and actuators. a: power supply for the MCU, b: communication bus, c: power supply for solenoids, d: pressure supplies.	30
4.4	Circuit board design and a prototype PCB. The chip on the top left is the MCU, the chip on the bottom is the IO expander. Three dual H-Bridge chips locate on each edge of the PCB.	31
4.5	A wrist performs fully compressing (A), fully stretching (B), and bending to different directions (C1) to (C6). The circuit design and wire arrangement are slightly different from the one shown above.	32
4.6	Rendered soft robotic arm made of three wrists.	33
4.7	An arm with two wrists demonstrates the state of (A) fully contracted, (B) fully stretched, (C) two modules bend towards the same direction, (D) and two modules bend towards opposite directions. Comparing (A) and (B) one can see the length of a fully stretched arm can double its contracted length.	34
4.8	A three-section arm controlled by ISTR protocol.	35
4.9	The sequence of data sending to and collecting from the modules.	36
4.10	Timing Diagrams of ISTR protocol.	37
4.11	Sequence of sending and receiving data of all sections on a four-section arm. One MCU starts repeating/appending data immediately after finishing its own part, minimize the delay as a relay, thus reduce the latency of modules near the end effector on a long arm.	37

List of Abbreviations

DoF	Degree of Freedom
PAM	Pneumatic Artificial Muscle
DEA	Dielectric Elastomer Actuator
EAP	Electro Active Polymer
IPMC	Ionic Polymer-Metal Composites
EMPV	Embeddable Micro Pinch Valve
LTC	Local Three-state Controller
IIC	Inter-Integrated Circuit
USART	Universal Synchronous/Asynchronous Receiver/Transmitter
ISTR	Isomorphic Synchronous Transmit-Receive

Chapter 1

Introduction

1.1 Soft Robot

Robots can be classified as hard or soft depending on the materials they are made of. Conventional manufacturing robots are made stiff so that they are powerful, precise and productive for stream-lined work. However, most situations in real world are not as organized as they are in factories. The tasks in real situations usually require safer and more versatile robot-object or robot-human interfaces, and better adaptability to different terrains and unpredictable obstacles. These raise the need for soft robots that are less rigid, using materials similar to the mechanical compliance and versatility of the materials and organisms in nature.

Soft robots are designed for handling tasks that are difficult for rigid robots. Taking the advantage of soft materials, the performance of a simple soft structure may outclass a complex rigid counterpart in certain tasks, e.g. picking up delicate objects of different shapes and sizes that are contaminated in an accident. Comparing to the robots used for manufacturing that are composed of rigid components like steel bearings, magnets, copper wires and steel frames, soft robots are made out of soft and extensible materials that can deform and adapt to the geometry of objects and absorb much of the energy arising from a collision. This makes them intrinsically safe to the surrounding and human, without many additional sensors.

The technologies of robotics and automation are demanded for nuclear facilities and other radiation-involved environments [1]. Universal robots for handling radioactive material and contaminated objects are essential for both regular operations and unexpected circumstances [2]. Developing soft robot capable of working in different terrains and handling different objects helps preventing harm to human workers in these situations.

The field of soft robotics is evergrowing [3, 4]. There have been many designs on different soft actuators [5, 6] and soft sensors [7, 8, 9], and meanwhile control theories for soft, continuous system are being developed [10, 11]. The major difficulties are how to build soft actuators as powerful as our muscles, and how to make sensitive and reliable soft sensors, and how to control the unconstrained structure of the soft body.

My work in this thesis relates to soft actuators and the implementation of them in soft robots.

1.2 Soft Actuators

There are majorly three types of actuators used in soft robots, which are fluid-driven actuators, EAP-driven (EAP: electro active polymer) actuators and SMA-driven (SMA: shape memory alloy) actuators.

Fluid-driven actuators are powered by either pneumatic force or hydraulic force. A fluid-driven actuator has one or many expendable cells, the volume of which changes with the applied pressure. The behavior of the entire actuator can be programmed by adding confinement to the actuator body, e.g. PneuNets actuators (Figure 1.1) add a non-stretchable layer next to the cells so that the actuator will bend when the cells are pressurized [12]; Fiber-reinforced actuators use non-extendable wires wrapping around the single-cell body and can achieve different deformation with different wrapping pattern [13, 14, 15](Figure 1.2). These actuators are easy to fabricate with liquid rubber and customized molds, and they can be made into large sizes. Usually the operating pressure is several kilo Pascal above the atmosphere pressure.

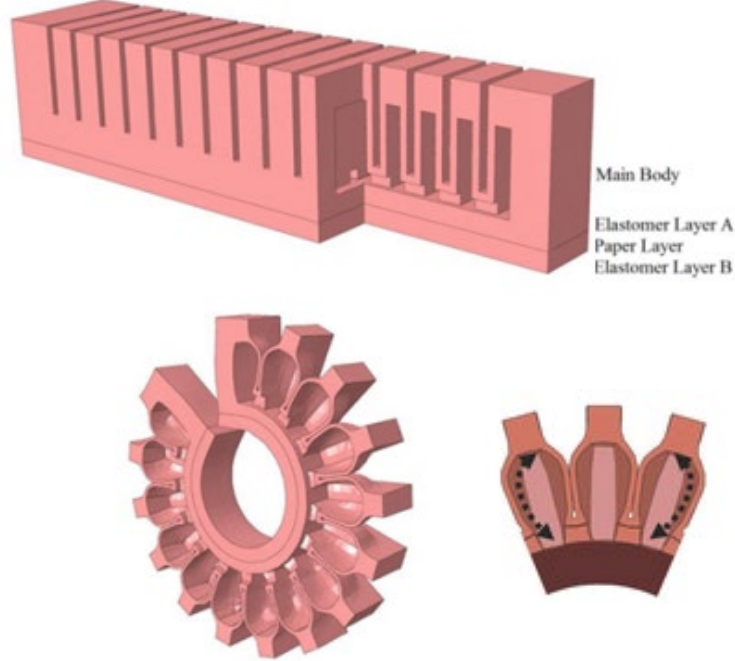


Figure 1.1: PneuNets Bending Actuator by Whitesides Research Group, pictures taken from Ref[12]

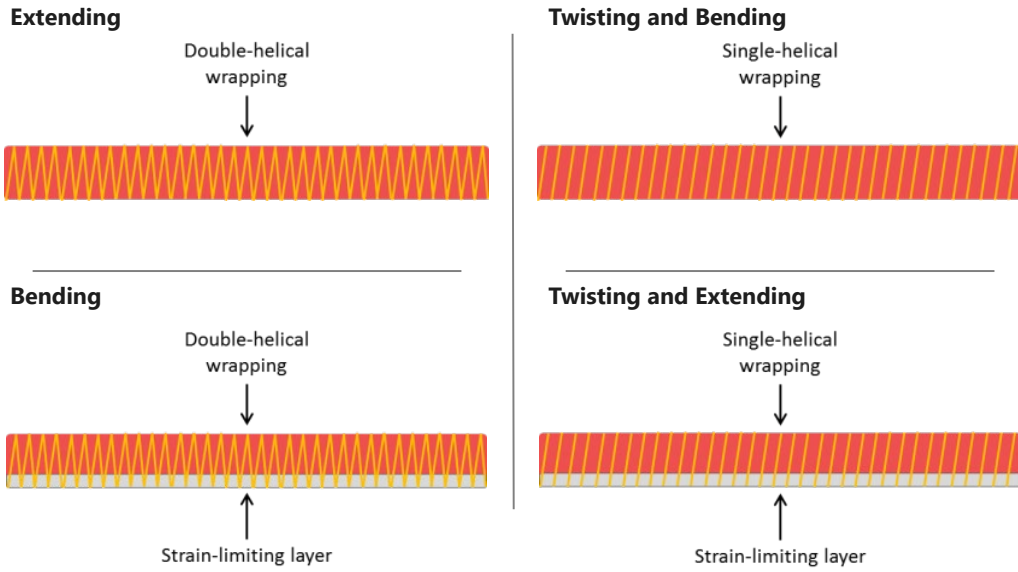


Figure 1.2: Fiber-Reinforced Actuators, pictures taken from softroboticstoolkit.com

EAP-driven actuators use electric force to create deformation. There are two types of material being used: dielectric elastomer and ionic polymer-metal composites. Respectively, dielectric elastomer actuators (DEA) have a capacitor-like structure with a soft insulation elastomer membrane placed between two compliant electrodes. When a voltage is applied to the electrodes, the attraction of different electric charge decreases the thickness and increases the area of the membrane [16, 17].

Ionic polymer-metal composites (IPMC) [18] actuators use the principle that ions move in the electric field. The polymer contains metal cations that can move freely, and when an electric field is applied to the material, the cation will move to electrodes with the surrounding water. The difference of the concentration leads to different inner stress, results in a bending shape (Figure 1.3).

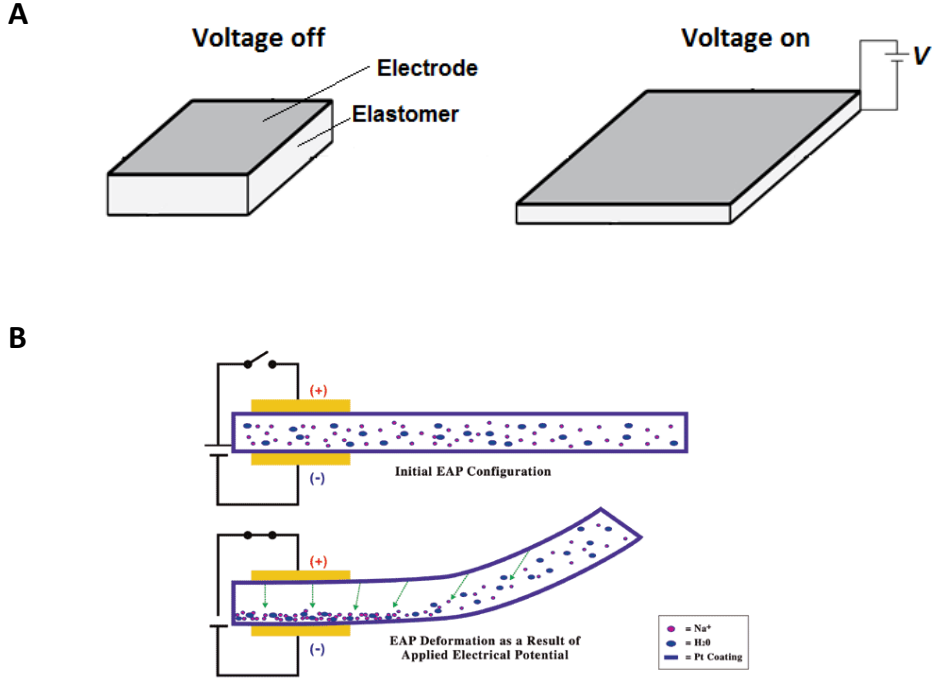


Figure 1.3: (A) DEA, pictures taken from Ref[17] and (B) IPMC, pictures taken from Ref[18]

SMA-driven soft actuators are the only metal-based actuators. They are made of nickel alloy that are relatively soft and easy to deform under external force at room temperature. When heated up, the alloy will undergo a phase change and restore its elasticity, changing back to its programmed shape. Usually the temperature is controlled by ohmic heating. The phase-change temperature is determined by the alloy type and composition and can vary between -150°C and 200°C .

Both EAP-driven actuators and SMA-driven actuators are controlled directly by electric power, and it sounds promising as the electrical components are simpler for design. However, DEAs need high voltage to operate, usually several kilo volts to generate adequate force and deformation; IPMC uses a regular voltage of 4-7 V to deform, but it cannot generate enough force in a small volume. The resistance of SMA wire is low, so according to Joule–Lenz law, the current consumption is huge to heat up the actuator. Also, hot items in the surrounding can mistakenly trigger the deformation, and the response time of SMA is generally long, especially during cooling-down process [19].

As a result, using fluid-driven actuators is still the most practical approach to study soft robotics. They can be made larger and are more powerful comparing to other two types of actuators, so they are used in most soft robots that show practical applications [20, 21, 22]. Also, the material used to fabricate these actuators are safe to human, without poisonous components and electric hazard. These make them the most

ideal candidate for building environmental and human-friendly robots.

1.3 Fluid-driven Soft Robot

Controlling fluid-driven actuators generally involves compressors, valves and fluid channels. Soft robots built by such actuators are usually tethered by bunches of tubes that connect every actuator to a valve behind the scene like a marionette [23, 24, 25] (Figure 1.4 (A), (B)). The tubes become a problem when more actuators are added to a robot and the size of the robot needs to be optimized. Tubes are less flexible comparing to the actuators, as they cannot change in length and can only bend within the limited radius. If several tubes are packed together, they become even rigid. Using narrower tubes allows more tubes to be packed in a certain space, but the action speed of the robot will decrease significantly since the flow rate under the same pressure is proportional to d^4 (d is the inner diameter of the tube) according to the Hagen–Poiseuille law. Flexible thin-wall tubes are prone to bending and have low pressure rating. The problem of the tube is a challenge for the development of soft robots.

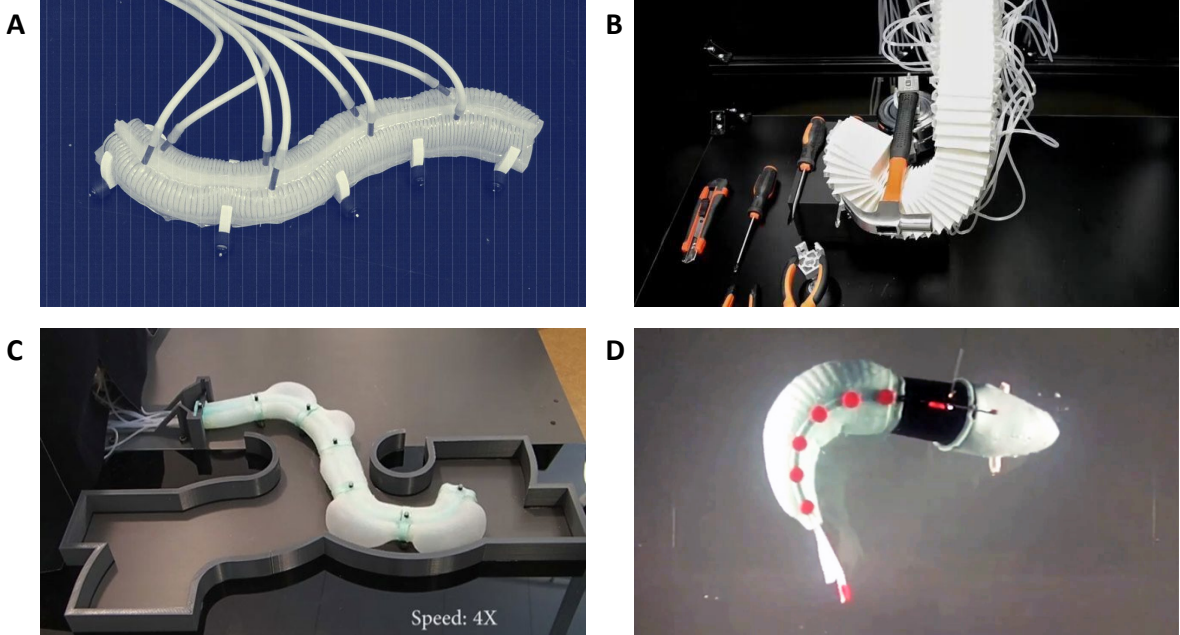


Figure 1.4: Soft robots made in labs. (A) A tethered soft robot worm by WPI Soft Robotics Lab; (B) HPN Manipulator by Jiang et al., picture taken from Ref[25]; (C) 2D-soft arm by Robert et al, picture taken from Ref[26]; (D) 1-DoF robotics fish by Andrew et al, picture taken from Ref[27]. Except robots with less DoFs (e.g. (D)), most fluid-driven soft robot are tethered by tubes.

Increasing the DoF is necessary for soft robots to complete complex tasks. For a soft robot made of linked sections, e.g. soft robotic arms, there are designs that all the tubes are fixed in the center axis [26] (Figure 1.4 (C)). This kind of soft robotic arms have fixed length with one or two DoFs for each section, so the tubes only need to bend with the arm. Some other designs arrange the tubes in a zigzag shape [25], allowing elongation and contraction along the axis. In either design, the existence of the tubes will influence the performance of the robot. When a new section needs to be appended to such arms, numbers of additional tubes that go through the entire arm to reach that section from the base have to be arranged. This is not scalable in terms of DoFs.

Unlike traditional robots that each DoF is controlled locally by motors, soft robots rely on valves that are hard to be built into the soft body. Simple robots carrying valves and pressure source are made in recent years, e.g. Andrew et al. built an autonomous soft robotic fish with one degree of freedom, carrying control circuit, valves and a miniature CO₂ cylinder inside [27] (Figure 1.4 (D)); Michael et al. made a large, untethered soft robot with four 1-DOF legs that carries both valves and micro air compressors [28]. These robots have less degrees of freedom, and control components take a large part of the robot.

1.4 Modular Soft Robot

Modular robot design enables fast assemble and easy repairing. It also allows modifying the robot structure according to the specified task on the fly. There are many modular designs seen in conventional robot field [29, 30, 31], but very few for soft robots. A modular component should only have supply and communication connections, all the functional parts within the module should be controlled locally. If the controllers for soft actuators locate outside the robot, any modification of the robot assembly will result in rearranging the tubes. So, the starting point for modular soft robot is to localize the control.

Robertson et al. designed a vacuum-powered modular soft robotic arm that several identical modules are linked together using an arterial vacuum supply[32] (Figure 1.5). Each module has three actuators, the vacuum supply tube is fixed in the center axis. The vacuum is distributed through three valves next to the actuators. This robot demonstrated the idea of a local pressure distribution system. Alex et al. designed a squeezing fluidic valve using electric field stress generated by liquid metal electrodes[33], which shows the attempt to locally control the pressure of the actuators, however the operation voltage is 5kV, which cannot be controlled directly by integrated circuit, and the overall size of the valve is not small enough to be implemented on every actuator yet.



Figure 1.5: Modular soft robot designed by Roberton et al., picture taken from Ref[32]

To address the problem of local fluid control, we designed the Embeddable Micro Pinch Valve (EMPV) which is light, small and simple while capable of controlling the pressure of the actuators locally with regular voltage (5V). Instead of blocking the pressure directly, an EMPV controls the cross-section area of the flow channel to manipulate the flow by squeezing the tube from outside. This principle has been wildly used in medical systems, food industries and drinking fountains due to its absolute isolation and zero dead volume. No part of the valve is directly exposed to the pressure, and no sealing is required for the shell of the valve, so the valve can be easily embedded into the robot, by either 3D-printing or molding.

All the EMPVs are connected to arterial pressure supplies, and locally control the pressure of the actuators. When the number of DoF increases, new actuators are appended to the artery through EMPVs, so no extra tube is required. This solves the problem that the number of tubes grows with increasing number of actuators. To demonstrate the capability of the EMPV, several 3-DoF modular soft robot wrists is built, each one uses 6 EMPVs. Then the wrists are connected together to act as a soft robotic arm.

Chapter 2

Embeddable Fluid Controller

2.1 Embeddable Micro Pinch Valve

EMPV is designed for locally controlling the fluid-powered actuators with minimal additional weight and size. The basic working principle of the EMPV is squeezing or releasing a soft tube according to the voltage applied to it. Traditional solenoid can be made in small sizes and controlled by low-voltage integrated circuits while capable of generating enough force to squeeze the tube. In comparison, ohmic-heating controlled SMA consumes a large current due to its low resistance, and the DEA requires a high voltage to generate enough force. Because neither high voltage nor large current can be controlled by integrated circuit, miniature solenoid magnetic is the most suitable actuator for the tube squeezing task.

The prototype EMPV is made using the smallest off-the-shelf solenoid magnetic and a 3D-printed shell (Figure 2.1). The size of the prototype is $18\text{mm} \times 8\text{mm} \times 7\text{mm}$ (Figure 2.2) and the weight is less than 2.5g .

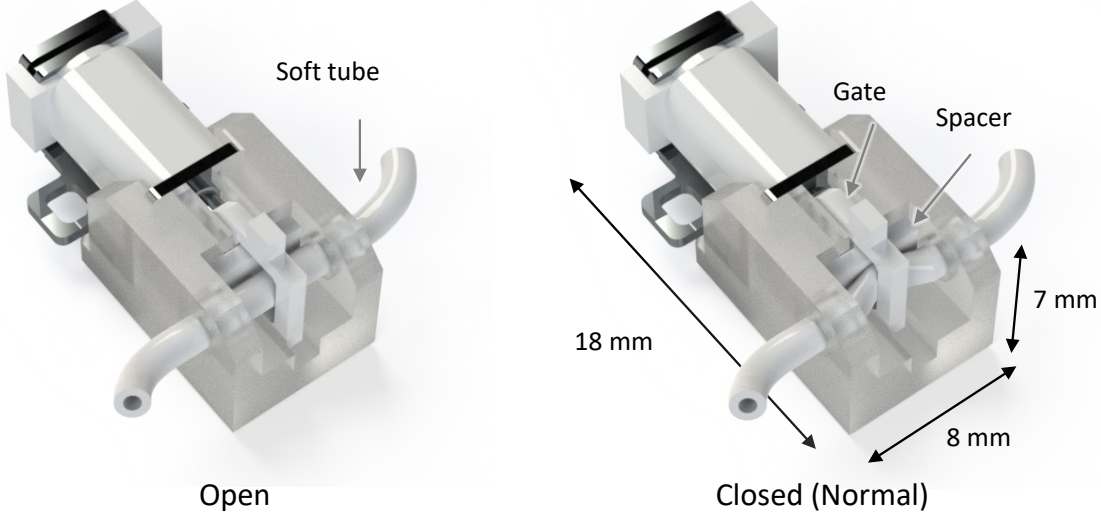


Figure 2.1: Basic structure and two states (open and closed) of the valve, close is the normal state.

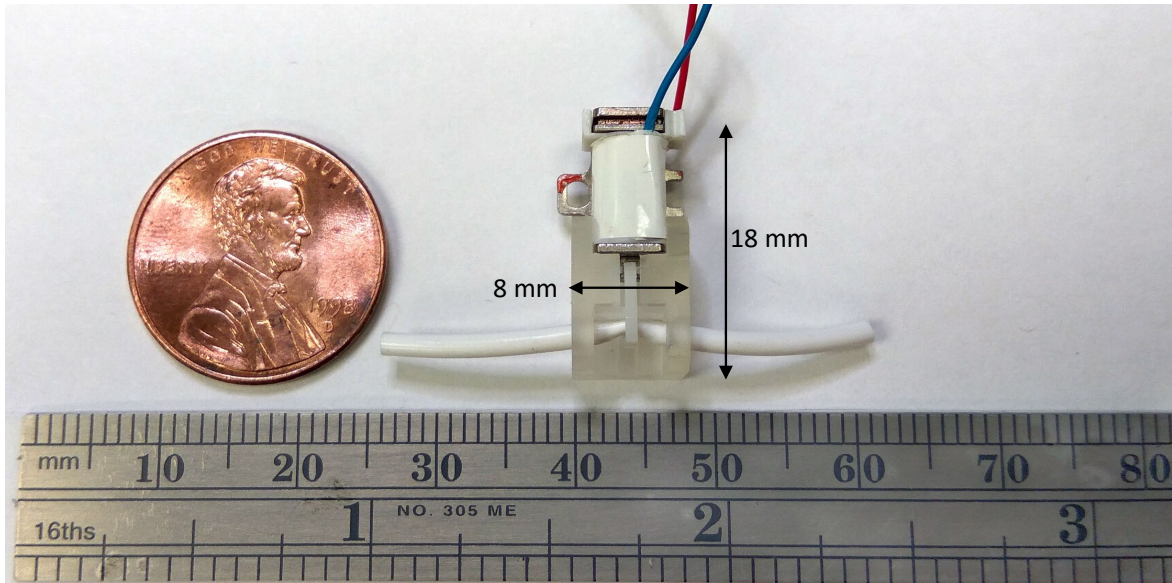


Figure 2.2: The dimensions of the EPV assembly.

The solenoid has a build-in neodymium magnet at its end, which normally attaches the steel plunger with a large force (900mN). This feature is utilized to keep the valve closed when there is no current in the coil, in another word, make the valve normally closed.

The plunger connects to a gate which squeezes the tube with a fixed spacer when the valve is closed (Figure 2.3). When a reversed magnetic field created by the energized solenoid cancels the magnetic field of the permanent magnet, the plunger is released. The gate will then open under the elasticity of the tube. The pressure difference inside and outside the tube plays an important role in this process, which will be shown later.

A reverse current which strengthens the magnetic field can be used to generate larger force upon closing the valve. The attraction force from the permanent magnet decreases fast with distance, not sufficient to pull back the plunger after the coil is de-energized in most cases. In the prototype valve, we use a silicone tube with durometer 35A hardness and 1/32" ID, 1/16" OD, and it will block the plunger from returning to the shutoff position when the pressure inside the tube is higher than the ambient pressure. The magnetic field generated by the solenoid tends to attract the plunger to the center-aligned position, however the force near the balance position is small. The combination of the solenoid and the permanent magnet solve the problem because once the plunger is near the end, the force from permanent magnet is predominant. An integrated H-bridge can control the direction of current in the solenoid.

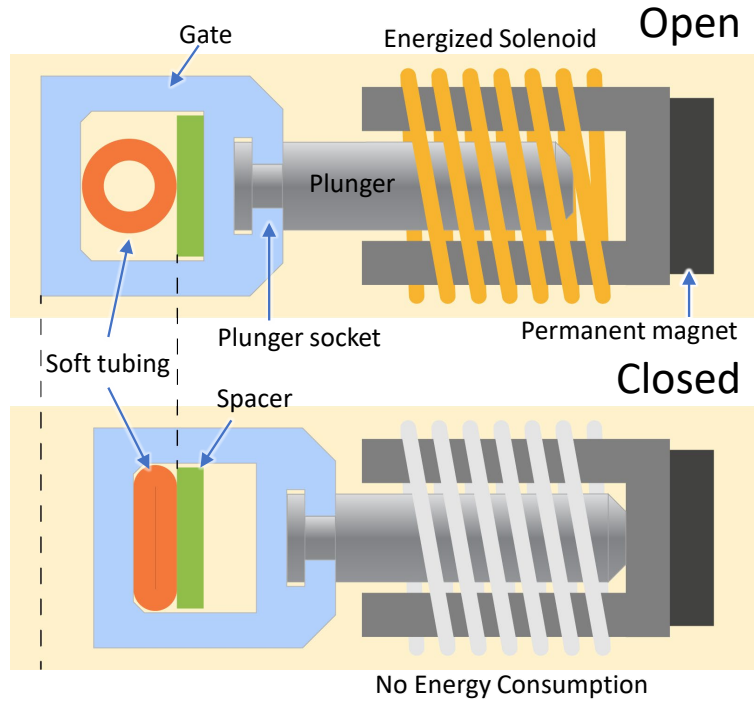


Figure 2.3: Schematic diagram of the working principle of the EMPV. The permanent magnet attracts the steel plunger in closed state. A reverse magnetic field generated by the energized solenoid can cancel the attraction and release the plunger, which allows the tube to recovery to its original shape by both pressure and elasticity.

2.2 Fabrication of the EMPV

The shell of the EMPV is printed by an SLA 3D printer (Formlab Form 2) with a layer thickness of $50\mu m$. The spacer and the gate are cut from resin sheet (Delrin Acetal Resin Sheets, McMaster-Carr, 8573K271) by a milling machine (Bantam Tools Desktop PCB Milling Machine). The tube used in all the prototypes is an off-the-shelf silicone tube (Durometer 35A, 1/32" ID, 1/16" OD McMaster-Carr, 5236K501). The 3 Psi maximum pressure given in the description is far below the burst pressure. The burst pressure is above 30 Psi (200 kPa) from lab measurements. For the pressure range we used in the prototypes (-100 to 100 kPa), the radial deformation is not noticeable.

The solenoid magnet is the off-the-shelf product brought on amazon. It is originally designed as electromagnetic brake. The neodymium magnet is built inside the solenoid. In cases where the size of EMPV needs to make even smaller, the support for bolts can be cut.

2.3 Squeezing Mechanism

The tube in the EMPV has to be soft and elastic to completely block the flow when it is squeezed and restore to normal shape when the force is removed. Silicone rubber tubing is good for this application. The burst pressure of the tube determines the burst pressure of the valve. The maximum operating pressure is determined by the squeezing force, which is then determined by size of the gap between the gate and the spacer when the valve is closed. The smaller the gap, the larger the squeezing force due to the compression of the elastic tube. The minimal force required to stop a pressure is:

$$F_s = F_e + F_p \quad (2.1)$$

, where F_s is the minimal squeezing force, F_e comes from the elasticity of the tube and F_p is the force due to the pressure difference inside and outside the tube. For the same tubes, F_e is determined by the width of the gate, while F_p is determined by the geometry condition after squeezing. We measured the minimal squeezing force under different relative operating pressure (Figure 2.4) and found the relation is linear for both positive and negative pressure, but the slope is different.

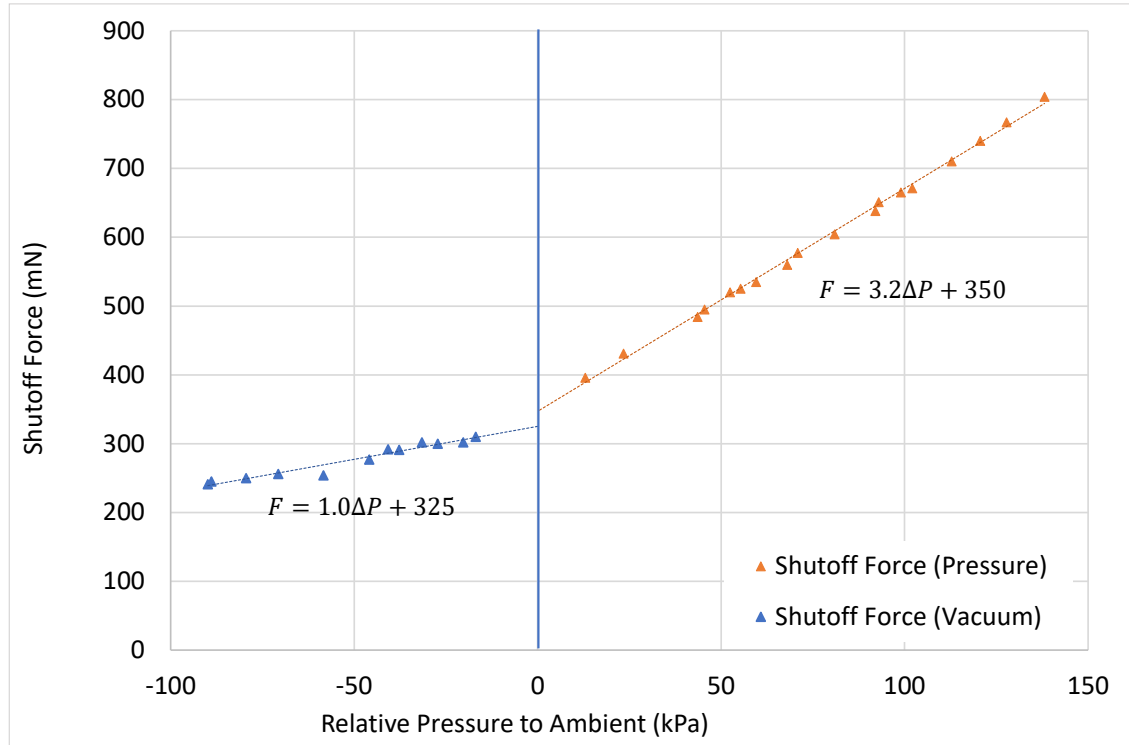


Figure 2.4: Closing force for different inlet pressure, relative to ambient.

An explanation for the slope crossover from negative pressure to positive pressure is as follow: Positive pressure tends to open the channel, so the tube must be completely squeezed by the gate, the higher the pressure, the larger the squeezing force is required; negative pressure, however, cannot close the channel on its own because the rest of the tube after the gate is connected to the ambient. It can help the gate with some force, but the ambient side will tend to open and let in the flow when the force on the gate is weaker than F_e .

This guarantees that as long as the negative pressure on both sides of the valve is not enough to collapse the tube, the EMPV will work. In fluid-control applications the negative pressure from the vacuum source is for exhaust, which means there is always a higher pressure on the other side. Thus, EMPVs are suitable for controlling tasks.

2.3.1 Squeezing Force Measurement

A test platform is designed and 3D-printed to tune the force of the gate (Figure 2.5). In this test, the gate is not connected to the plunger, but a force gauge (VTSYIQLI HF-5) instead. A bubbler is connected to the tube after the gate to indicate the existence of the flow.

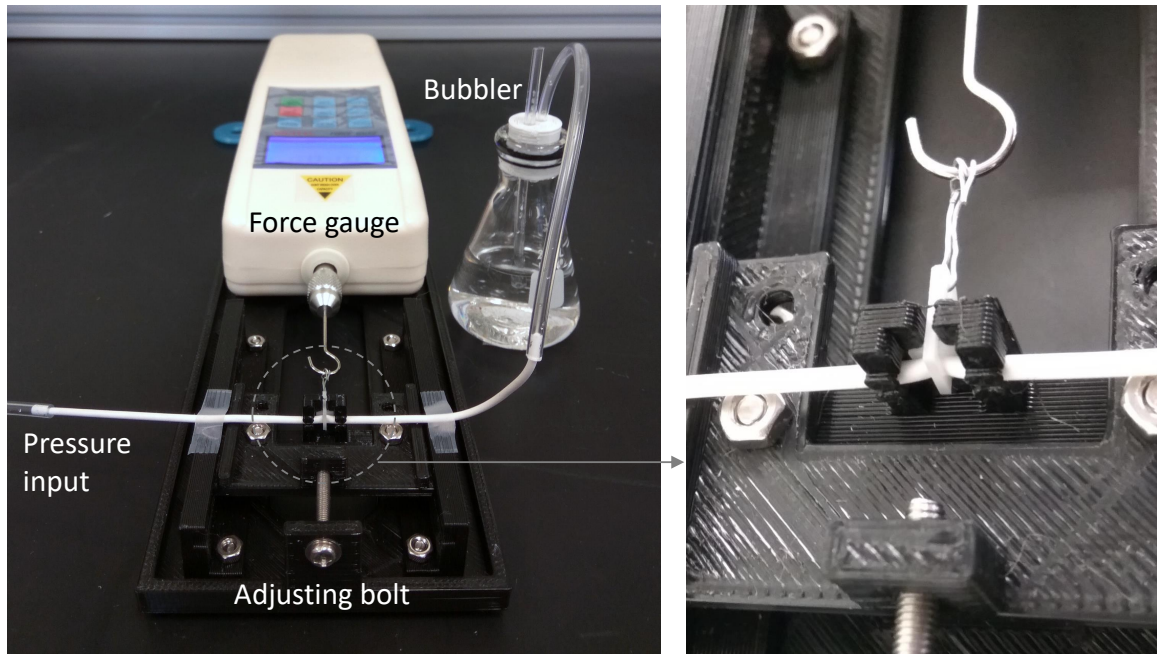


Figure 2.5: Experiment set up to measure the squeezing force

For positive pressure, the tube connects to the long tube of bubbler that goes below the fluid level;

for negative pressure, the tube connects to the short tube of the bubbler that stay above the fluid level. Changing of the fluid level inside the long tube or air bubbles coming out of the long tube shows the soft tube is not closed. In real practice, it is difficult to get to the point where the flow just stops, so the squeezing force is recorded when the leaking rate is slow enough (< 1 bubble in 10 s). All measurements are taken under room temperature.

2.4 Response Time of EMPV

The response time of an EMPV is influenced by the pressure difference inside and outside the tube. During the opening process, the tube opens the gate on its own, so the higher the pressure inside the tube, the larger the force opening the gate, results in shorter opening response time (t_o). When the outlet of the EMPV is connect to ambient, t_o decreases exponentially with the increasing of input pressure (Figure 2.6), and the relation is consistent for negative pressure from vacuum supply.

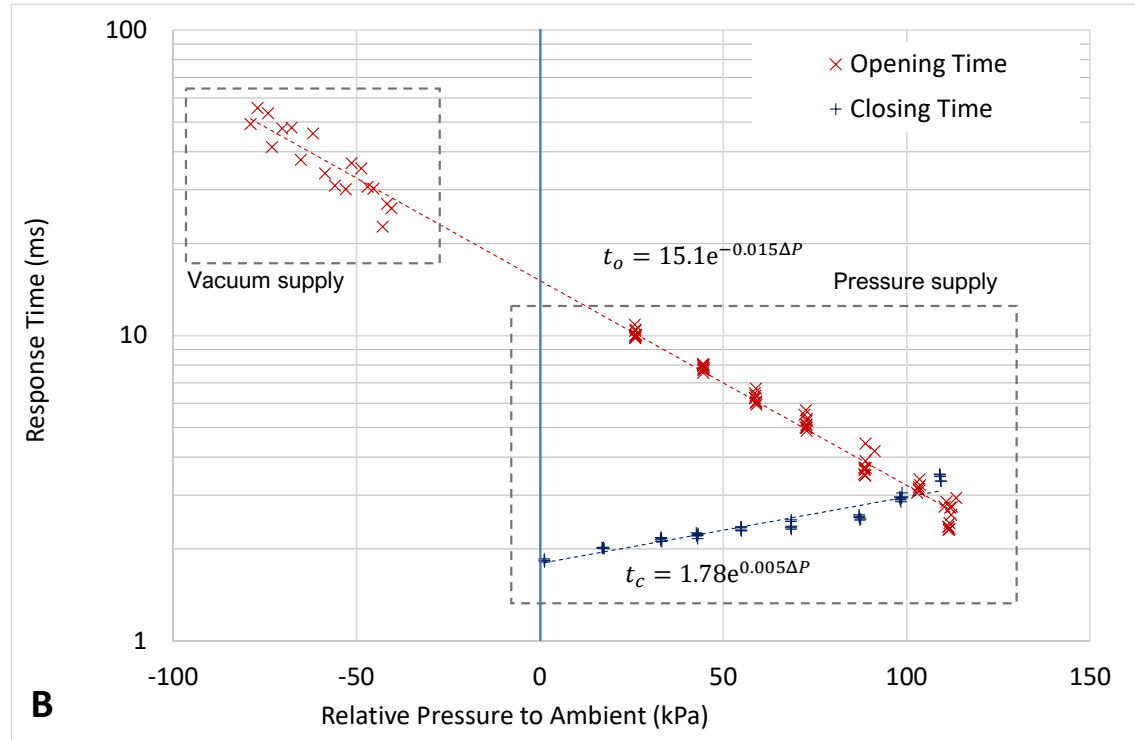


Figure 2.6: Response time for different inlet pressure

After applying voltage to the solenoid, there is a death time that the pressure does not change, after

which the pressure rises in a S shape. It also takes some extra time for the outlet pressure become stable (Figure 2.7). The response time is measured as the outlet pressure reaches 50% of the stable pressure during the rising stage, where locates the maximum flow rate (Figure 2.8).

During the shutoff process, the force generated by the solenoid and the permanent magnet is dominating, therefor the closing response time (t_c) is less affected by the pressure difference and generally faster (Fig. 2B). Unlike the opening process, shutting-off of the valve is not reflected by the changing of the outlet pressure, so the closing response time is measured by the second peak of $U_{solenoid}$, which marks the vanishing of the reverse voltage from the increasing of the magnetic flux when the plunger hits the end (Figure 2.9 and 2.10). The time for pressure dropping is decided by the exhausting speed, thus cannot represent the closing time properly. Below the ambient pressure the EMPV can shut off without the reversed current. Though this makes measuring t_c by voltage signal impossible, we can assume a response time not longer than the t_c under positive pressure. The relatively fast closing response ($< 4ms$) makes the valve capable of doing precise closed-loop control.

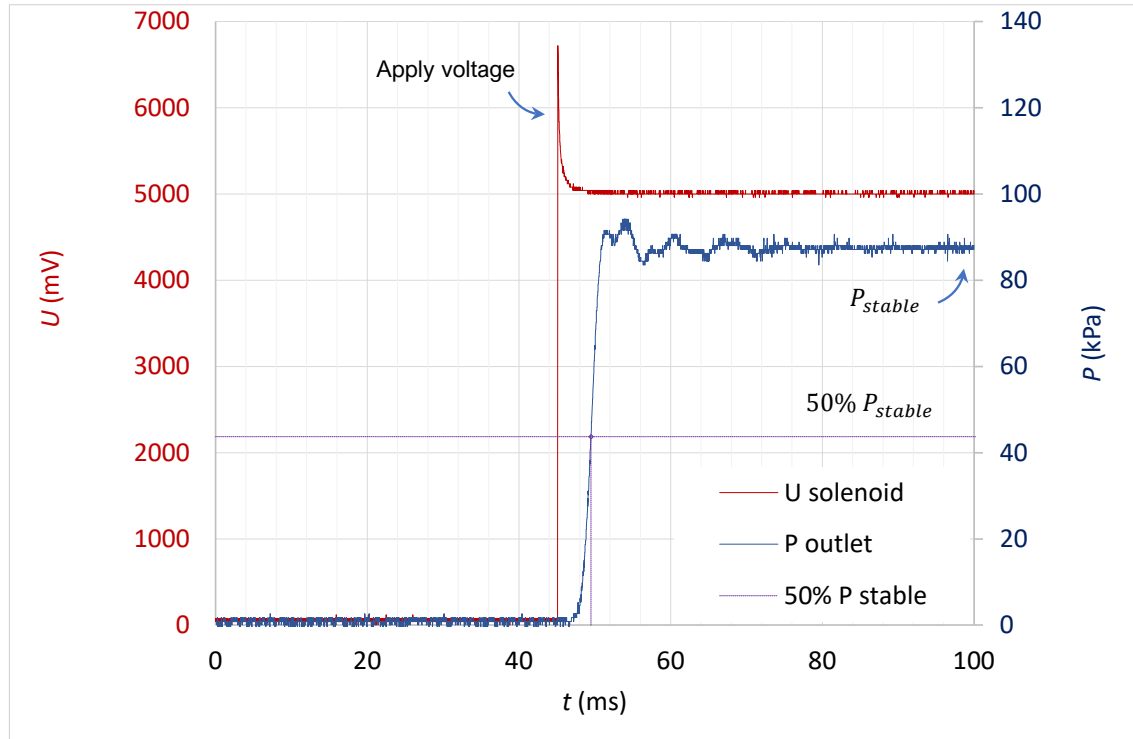


Figure 2.7: Typical response curve of energizing an EMPV

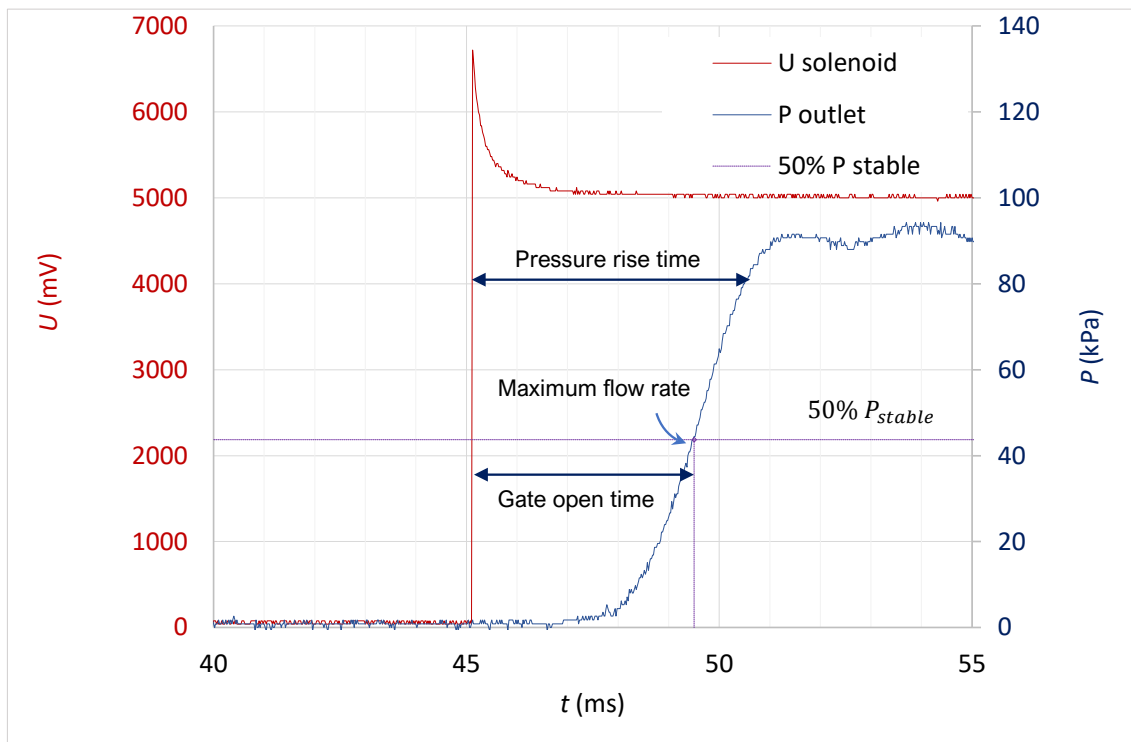


Figure 2.8: Detailed energizing process. The average opening time of the EMPV is 7ms.

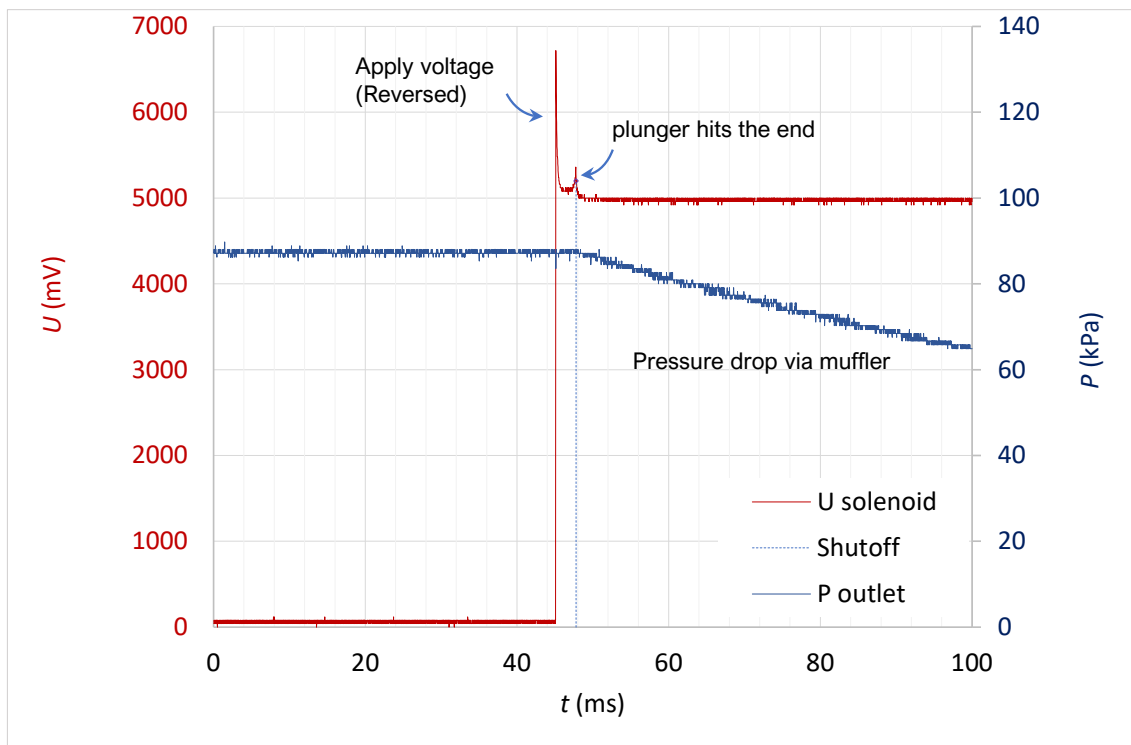


Figure 2.9: Typical response curve of closing an EMPV by reverse current.

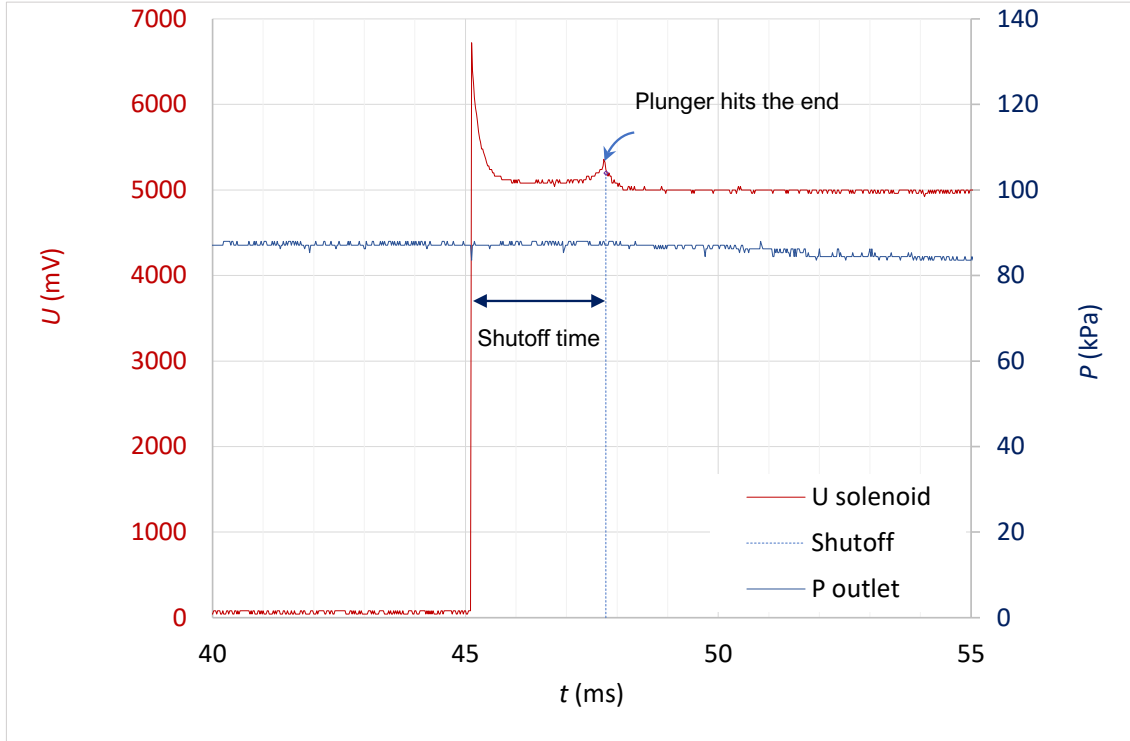


Figure 2.10: The details of closing process

2.4.1 Response Time Measurement

The response time above is measured by a pressure sensor (MPX 5500) and a duel-channel oscilloscope (OWON VDS1022I) (Figure 2.11). Channel 1 of the oscilloscope connects to the output of the pressure sensor, and channel 2 measures the voltage difference of the solenoid. The voltage supply for the pressure sensor must be completely isolated from the supply for the solenoid to avoid the strong interference when the solenoid is energized. The isolated 5V supply is acquired from a 7.4V Li-Po battery and a voltage regulator. A simple circuit including an MCU, an integrated H-bridge and two PID buttons are used to manually control the open and close of the EMPV. The MCU monitors the state of the button, erasing the jitters and control the input of H-bridge accordingly via I/O pins. This avoids the voltage spikes on the solenoid and smooth the outcome.

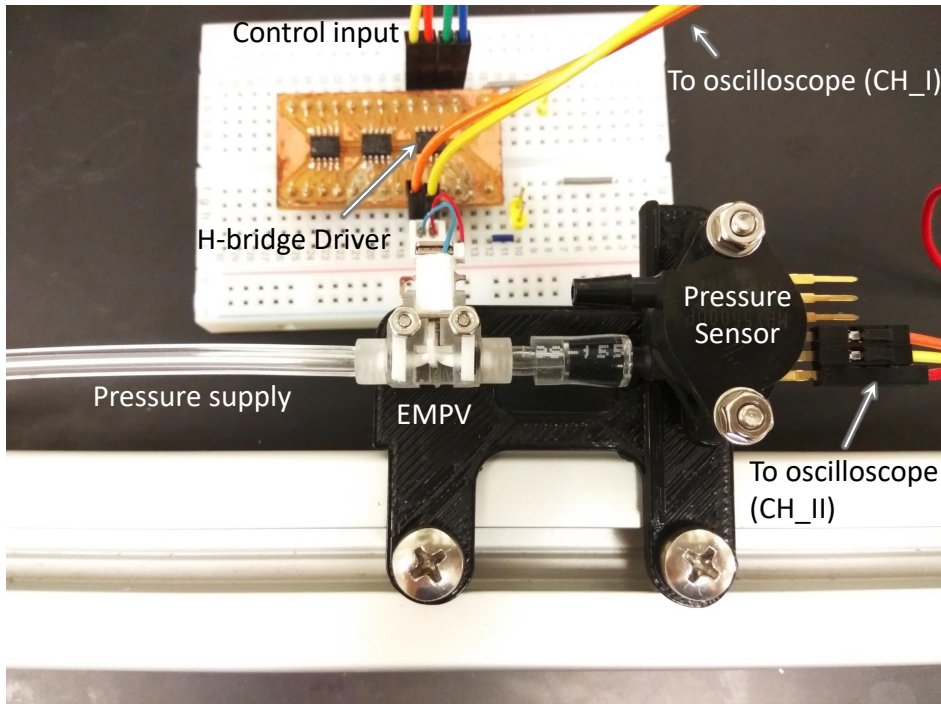


Figure 2.11: Response time measurement setup

The pressure sensor has two input, P1 and P2. The pressure applied to P1 should be greater than to P2. The voltage output from the sensor is linear to the pressure difference of P1 and P2, from 0kPa to 500kPa. The actual pressure difference in kPa is calculated by:

$$\Delta P = (V_{out}/V_s - 0.04)/0.0018 \quad (2.2)$$

, where V_s is the voltage apply to the sensor.

For positive pressure, a regulator is used to control the pressure applied to the inlet of the EMPV. A short tube connects the outlet to P1 while P2 opens to the ambient. A tiny hole is opened on the tube so that the pressure will return to ambient slowly after the EMPV is closed but will not affect the pressure readout during the measurement. At least six data are collected at each one of the seven different pressure ranging from 25 kPa to 110 kPa. For negative pressure, the outlet connects to P2. No vacuum regulator is available, so the measurements are scattered within -80 kPa to -40 kPa. There are twenty measurements in total for negative pressure. All measurements are taken under room temperature.

Chapter 3

Hybrid Actuator

A hybrid actuator is powered by pneumatic force but controlled locally by the EMPV according to the input voltage. It is the first step to make a modular soft robot. The following sections describe how a controllable hybrid actuator is made and its capability to be closed-loop controlled.

3.1 Local Three-state Controller

An actuator under closed-loop control should have three states: inflating, exhausting and holding pressure. Otherwise it can only be either maximum inflated or completely exhausted. A traditional solenoid valve with one solenoid only has two states: either open and close for 2-way valves, or pressure and exhaust for 3-way valves, because one solenoid can only have two positions. A three-state controller is designed by using two normally closed valves, one for inflating and one for exhausting. Since both valves are normally closed, the controller will hold whatever the pressure inside the actuator when there is no input. When the pressure needs to be changed, the valve connected to the pressure supply or the exhaust will open accordingly (Figure 3.1). By either reading the pressure inside the actuator or tracking the deformation, one can control its pressure to any certain value or set the deformation to any certain extent within the possible range. This is essential for modular design, since only supplies can go through the modules and all the actuators are linked in parallel to the supplies. Every actuator must be able to control its own pressure.

Three-state controlled actuators not only can be used in closed loops, but also improve the performance and energy efficiency of the robot. Actuators using only one valve are connected to the pressure source all the time when powered, so all the powered actuators will interfere with each other through pressure re-balancing. This process can even become unstable if the actuator does not react to the pressure linearly (Harnessing Snap-through Instability). Also, single-solenoid driven valves are mono-stable, the actuated state is kept by running current in the coil which only generates heat. With two normally closed valves, an actuator only consumes energy when the pressure in the actuator needs to change.

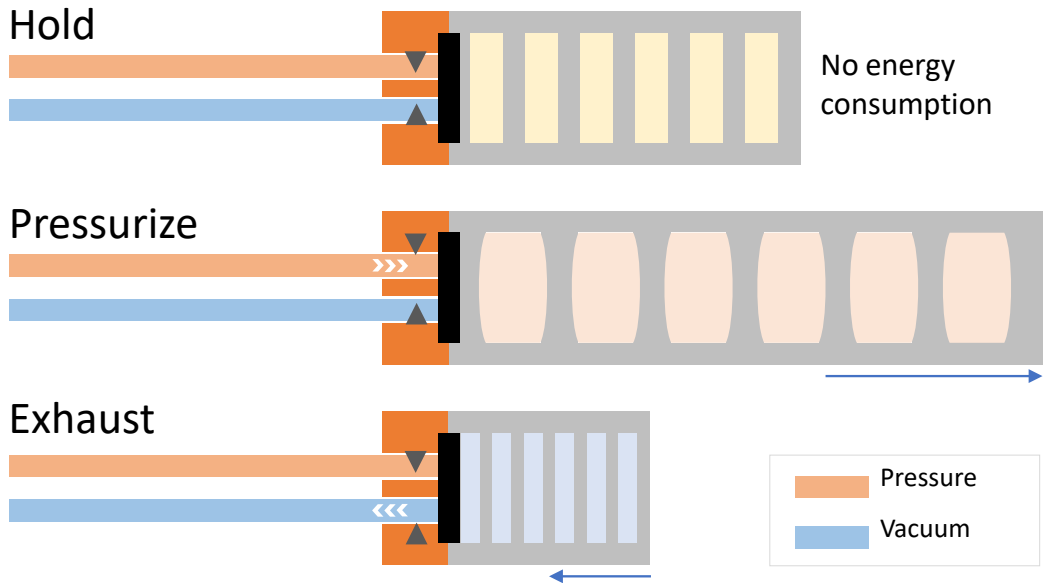


Figure 3.1: The working principle of three-state controller. Noting only when the actuator is changing its length does it consume current.

By using EMPVs, a three-state controller can be made in small size so that it can be placed locally with the actuator. A dual H-bridge driver controlling the EMPVs can also be built into the assembly. These create a local three-state controller (LTC), which will be used in the hybrid actuator.

3.2 Prototype Hybrid Actuator

A prototype hybrid actuator is made with one silicone pneumatic spring and an LTC (Figure 3.2). The frame of the valve, the channels and the connector to the actuator are all merged together and 3D-printed by resin as one piece. The EMPVs are assembled on the controller. The dual H-bridge chip connects to the controller via flexible flat cable (FFC) and manipulate the current in the solenoids .

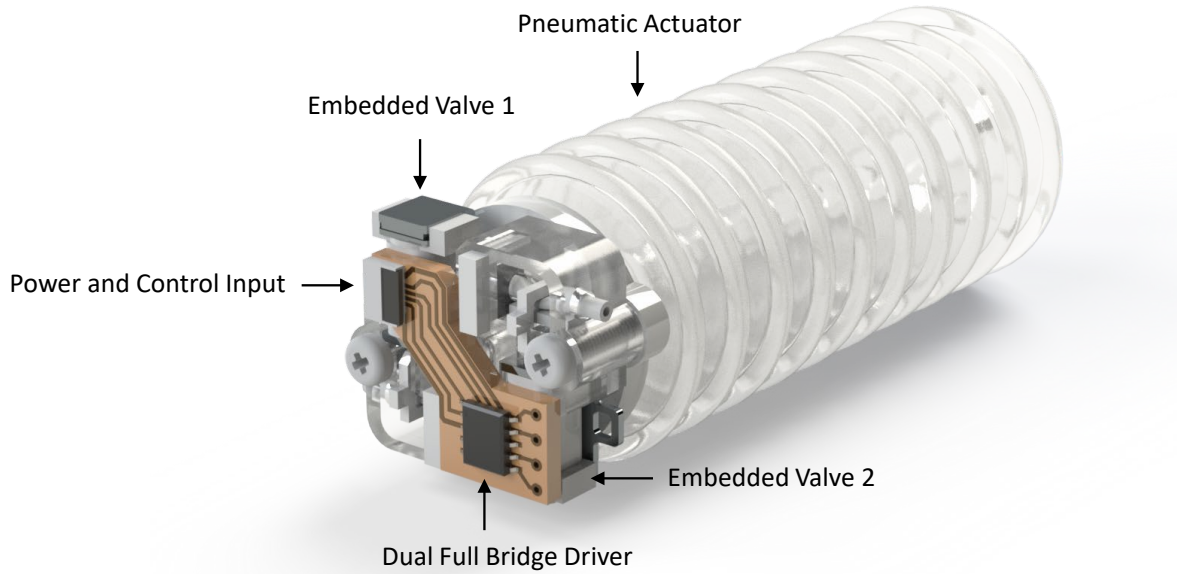


Figure 3.2: A rendered hybrid actuator. Two EMPVs are used to control the pressurizing and exhausting of the actuator. A dual H-bridge driver controls the polarity of the voltage applied to each EMPV according to the input.

The following subsections introduce how the hybrid actuator is made, including the 3D-printed LTC framework, fitting for soft tube, fabrication of the soft actuator and the fitting for soft actuator.

3.2.1 3D-printed LTC Frame

The frame of the LTC have the frames of both EMPV, and the EMPVs are assembled directly on the LTC (Figure 3.3). The frame also has built-in flow channel, connect the outlet of both EMPV to the soft actuator. A miniature fitting is designed to connect the tubes to the printed channels.

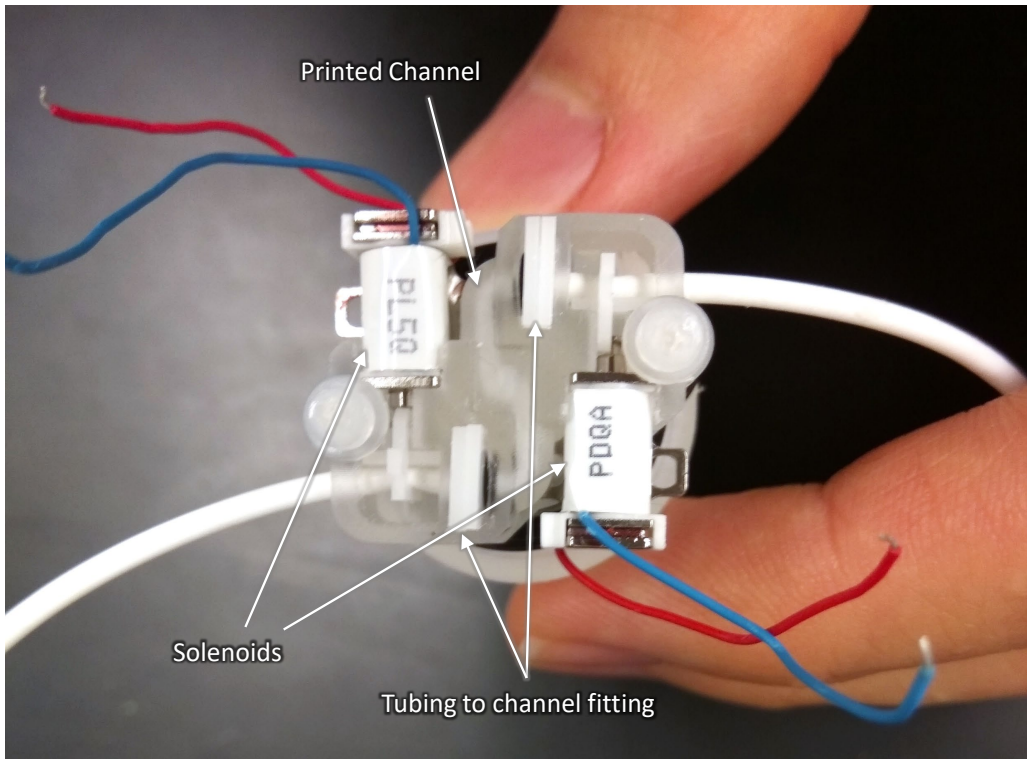


Figure 3.3: Actual LTC before mounting the local control circuit. The built-in flow channels can be seen in the middle of the frame.

3.2.2 Miniature Tube-to-channel Fitting

Since the outlet of the EMPV is the end of the soft tube, a fitting is needed to connect the tube to the channel. To minimize the space taken by the fitting, a structure similar to push-to-connect fitting is used. The fitting includes a 1/16' ID Buna-N O-Ring (McMaster-Carr, 9452K311), a washer and a push-in spacer. When the spacer is pressed into the fitting, it will push the wash which will then squeeze the rubber O-ring (Figure 3.4). This makes the O-ring thinner while its inner diameter will shrink. Because the original inner diameter of the O-ring is the same as the outer diameter of the tube, after squeezing it will lock the tube in place while sealing the gap between the tube and the channel. Both the washer and the spacer are cut from the same resin sheet used to make the spacer and the gate in the EMPV. The sealing can withstand the burst pressure of the tube.

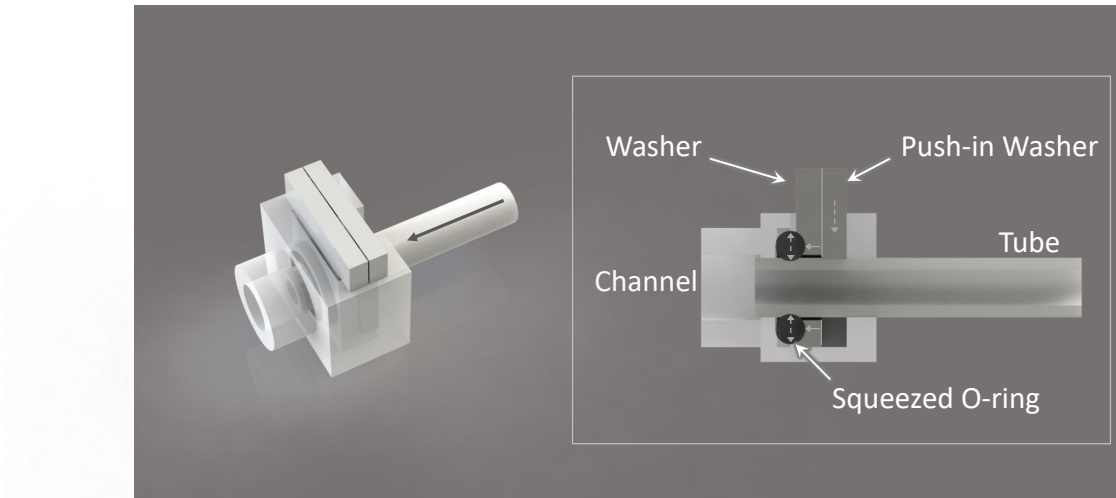


Figure 3.4: Miniature tube-to-channel fitting

3.2.3 Fabrication of the Silicone Pneumatic Spring

The soft pneumatic actuator on the prototype hybrid actuator is made of catalyzed liquid silicone rubber (Magikmold 6335 35A Clear Platinum Cure RTV Silicone). The pot life for the silicone is 90 minutes, and the cure time is 10 hours under room temperature. After mixing the liquid silicone with the catalyze, the mixture is degassed for 30mins and then pour into a three-piece mold. The mold contains two 3D-printed resin outer molds and one wax inner mold (Figure 3.5). After the silicone is cured, two outer molds will be removed, the inner wax mold will be melted, and the liquid wax will be recycled.

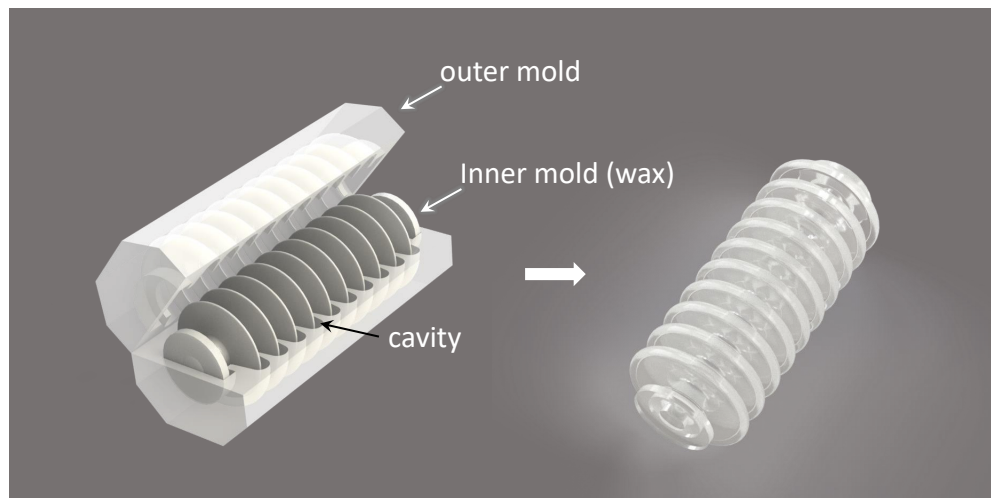


Figure 3.5: The molds used for silicone injection

The wax mold is prepared by another set of resin molds. The wax has a melting temperature about 56C, an incubator is used to keep the wax in liquid state during preparation. Because the wax is brittle after cooling down, the mold is made in small pieces (Figure 3.6) and assembled on a mold tray before injection. The liquid wax first fill-in the cavities on each half under room temperature, and then the two half-molds will be pressed together. Since wax is non-crystal, it remains soft for a while below the melting temperature, so the two half pieces can grow together. During demolding process, the mold is removed piece by piece so that it won't harm the structure.

The liquid silicone rubber can heal much faster at high temperature(30 minutes at 60 °C),but the use of wax inner mold makes it unfeasible.

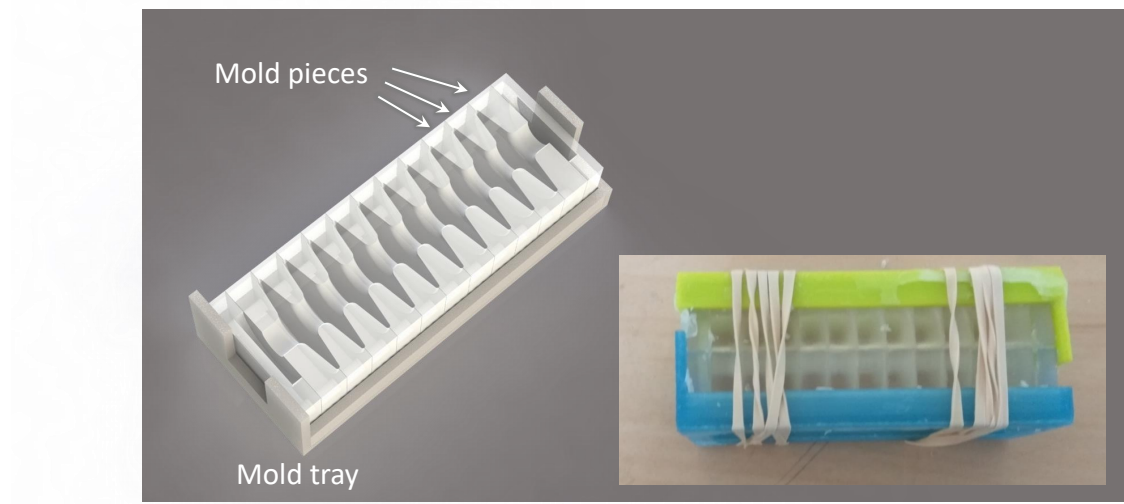


Figure 3.6: The molds used for the inner wax mold

3.2.4 Soft Actuator Fitting

The frame of the local three-state controller also has a fitting to the pneumatic actuator. The fitting is an extruded structure that goes into the actuator. The actuator has a neck structure that surround the fitting while being hold by a fixture. The fixture locks the actuator in place with two nylon bolts. Usually the silicone rubber is self-sealing, but in case the surface of the actuator has wax residues, an O-ring can be used to seal the fitting (Figure 3.7).

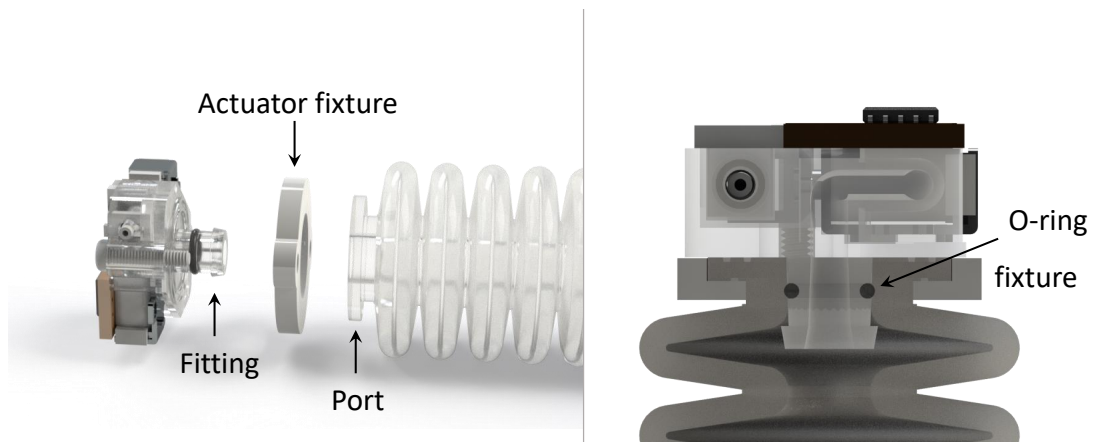


Figure 3.7: Fitting for soft pneumatic actuator

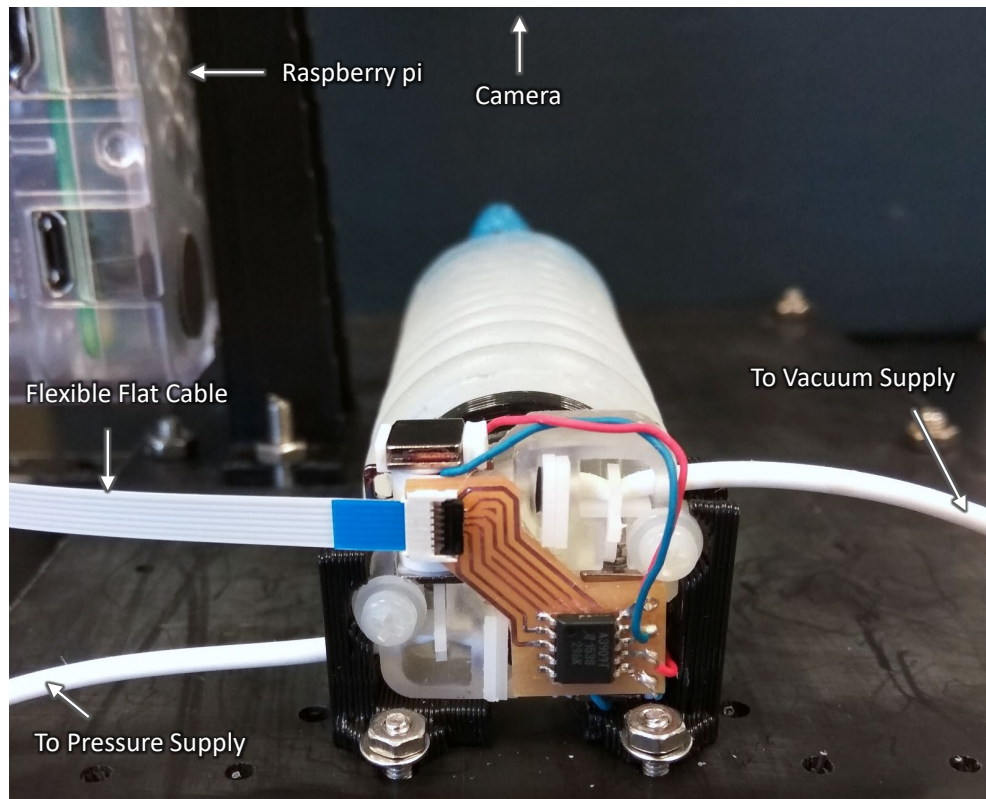


Figure 3.8: Connection to the hybrid actuator

3.2.5 Driver Circuit

The circuit board on the hybrid actuator connects wires from the solenoids to the dual H-bridge driver. The power supply and the input pins of the driver goes to a 6-position FFC adapter (Molex, 503480-0600). The prototype board is made with the PCB milling machine. In the following demo, an FFC connects the hybrid actuator to a Raspberry Pi (Raspberry Pi 3 with Pi camera) using an FFC to GPIO adapter (Figure 3.8).

The dual H-Bridge drivers used in all the prototypes and demos are A3909 chips from Allegro MicroSystems, LLC. The chip is designed for 12 V medium power applications. The outputs are rated for operation through a power supply range of 4 to 18 V, and capable of up to 1 A per phase. The operating voltage of the solenoid is 4 V to 6 V, and the coil has a resistance of 12Ω . The total on-resistance of the driver is 2.7Ω at 4 V, and it is smaller for higher voltage. This results in about 20% loss. To acquire a 5 V output, the input has to be 5.9 V. Figure 3.9 shows the schematic of the driver circuit and the board design.

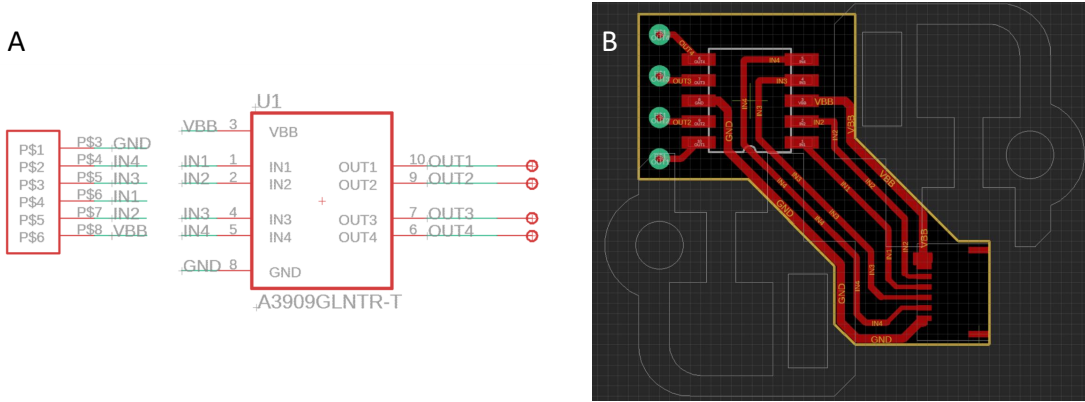


Figure 3.9: Driver circuit of the hybrid actuator. (A) Circuit schematic (B) Board layout

3.3 Feedback Control Demo

To demonstrate the controllability of the hybrid actuator, a closed-loop control is set up using camera feedback. The hybrid actuator is fixed to the ground and a camera from above will track the length of the actuator and a reference object (in this case a finger) and do a feedback control (Figure 3.10). Noting in all three pictures the actuator is in hold state, both EMPVs are in closed position, consume no energy. The small response latency is compensated by acting ahead of time according the measured deformation speed.

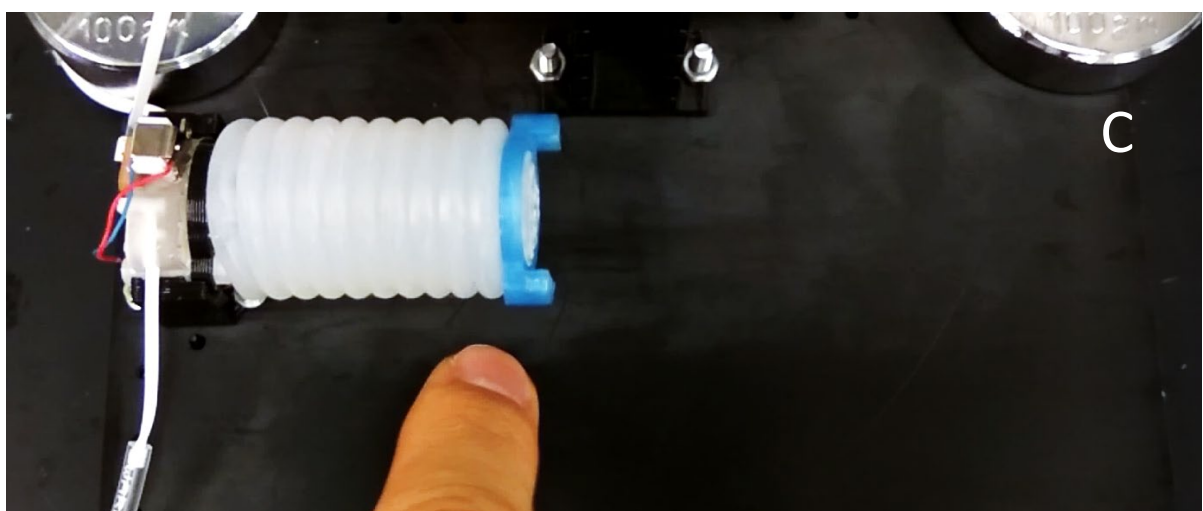
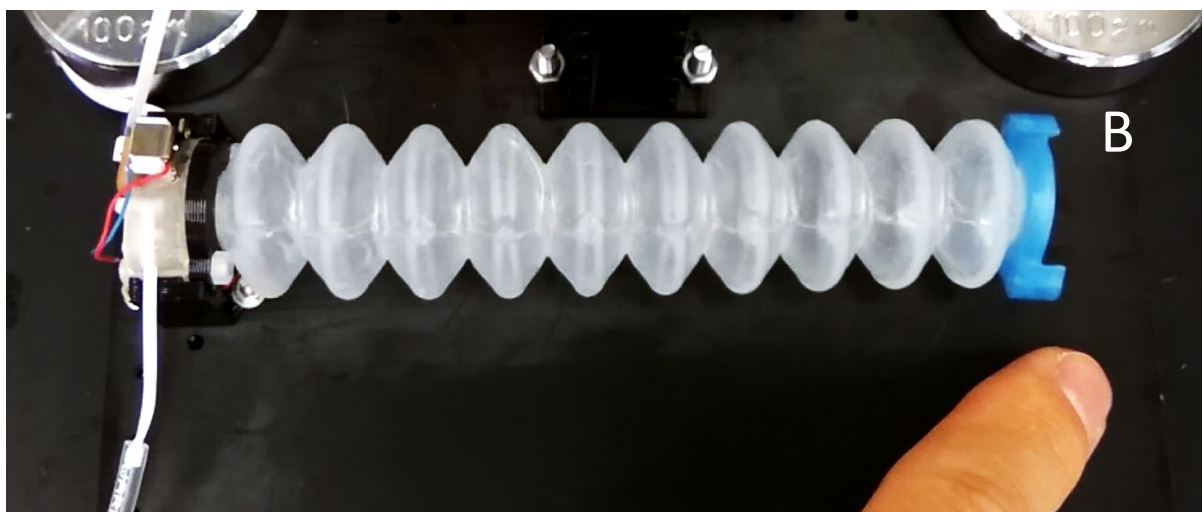
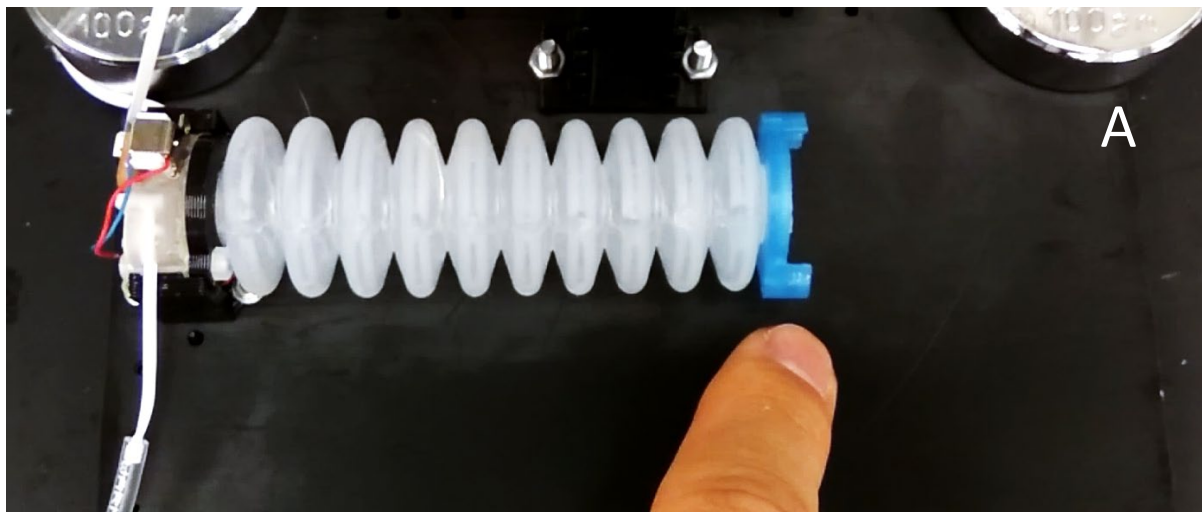


Figure 3.10: Feedback control demonstration, noting in all (A) to (C) the actuator is in hold state (No energy consumption).

The Pi camera is fixed 15cm above the actuator, so it can capture the whole actuator even when the actuator is at its maximum length (Figure 3.11). The Raspberry Pi searches the end of the actuator and an object next to it by thresholding. Then it compares the location of the object with the length of the actuator, and decides whether the actuator should inflate, deflate or hold still. There is a small displacement tolerance for the object to avoid oscillation.

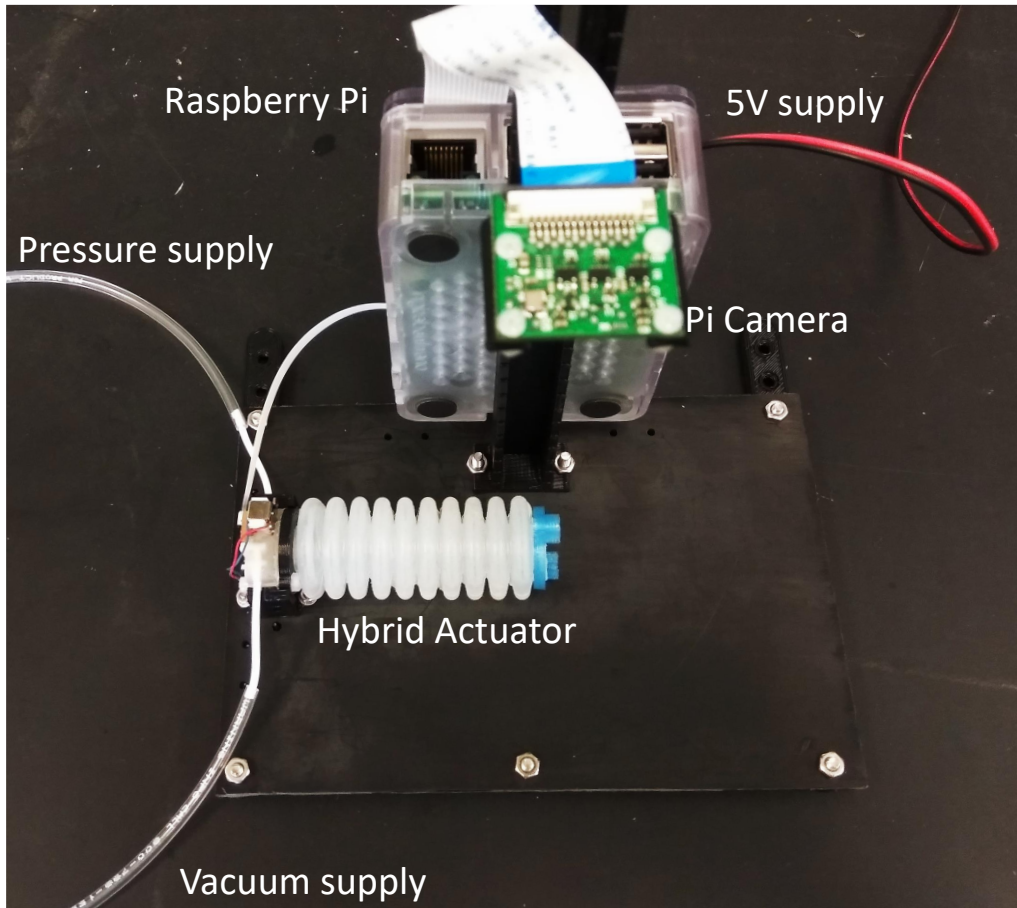


Figure 3.11: Connections and experiment setup.

Chapter 4

Modular Soft Robotic Arm

4.1 Modular Design

With locally controlled hybrid actuators, designing modular soft robots becomes possible. A modular soft robot consists of multiple modules that function individually. Such a design allows robots have different configurations for different jobs and enables easy repairing and modification. An individual module should have one or more degrees of freedom. To implement multiple degrees of freedom into one module, one can either combine several LTCs to drive one actuator with multiple chambers or binding several hybrid actuators together. In either way, a module should only have control input and pressure supplies, and it should be capable of connecting to other modules with uniformed connectors.

As a demonstration, we designed a 3-DoF modular soft robotics wrist consisting three independent hybrid



Figure 4.1: A 3-DoF modular wrist made of three hybrid actuators with low-profile TLCs (rendered).

actuators with low-profile LTCs (Figure 4.1). Instead of placing the EMPVs along the axis, low-profile LTC have both EPVs placed next to the actuator so that the non-extendable length (dead length) along the axis of the hybrid actuator is minimized and provide better heat dissipation. The wrist is designed to connect to other identical wrists to form a soft arm.

Besides the three hybrid actuators, some supportive structures and a local controller are included in the wrist. Figure 4.2 shows the top view and the side view of a wrist. A dual-channel three-way pressure distributor (7) splits the pressure supply and the vacuum supply for each hybrid actuator. Male and female pressure connectors (8,13) locate on each end of the wrist. Two arterial tubes let the pressure and vacuum

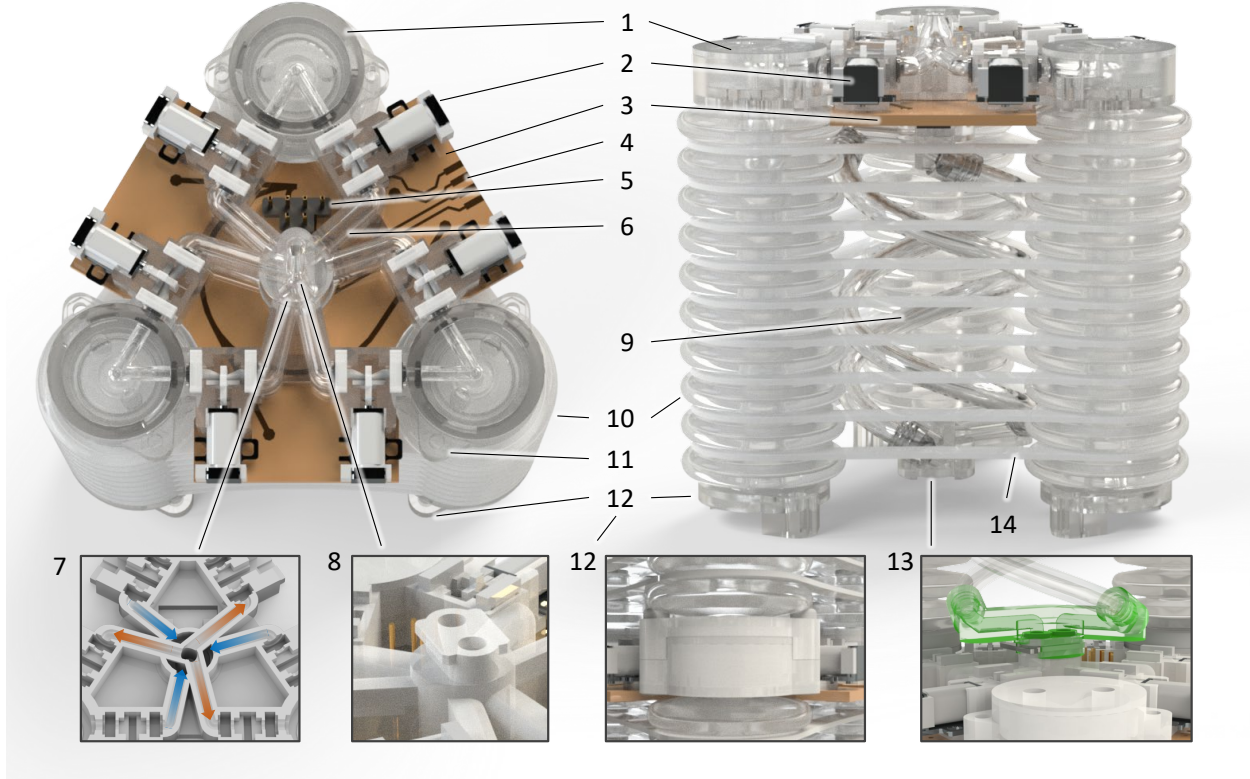


Figure 4.2: Instead of placing the EPVs along the actuator axis, low-profile LTC have both EPVs on the side, providing better thermal dissipation and consuming less space along the actuator. (1) Actuator fitting, (2) EPV, (3) circuit board, (4) programming pins, (5) communication header, (6) printed flow channel, (7) Printed three-way dual-channel pressure distributor, (8) Dual-channel pressure supply connector, (9) Arterial supply tubes in double helix shape, (10) Actuator, (11) Connector to previous section (12) connector to next module. (13) pressure connector to next module. (14) Vertebra plates confine the deformation of the actuators.

supplies go through the wrist in a double-helix shape (9). Mounting holes also added the hybrid actuators so that multiple hybrid actuators can connect to each other end-to-end (11,12). Since the three actuators are independent, vertebra plates are used to confine their relative position (14). All the circuit components, including the H-bridges of hybrid actuators, are placed on a single PCB (3). A micro control unit (MCU) on the circuit board communicates with other modules using serial protocol.

4.1.1 Control Circuit

The wrist is controlled by the single circuit board. As an individual functional module, it should be able to receive commands from a central controller and locally control all the actuators instead of having all the actuators directly linked to the central controller. Figure 4.3 shows the control hierarchy of a modular wrist. The MCU receives command from a data bus and controls the three dual H-Bridge drivers by its I/O pins. A total number of 12 outputs are needed since each H-Bridge requires two individual inputs to control.

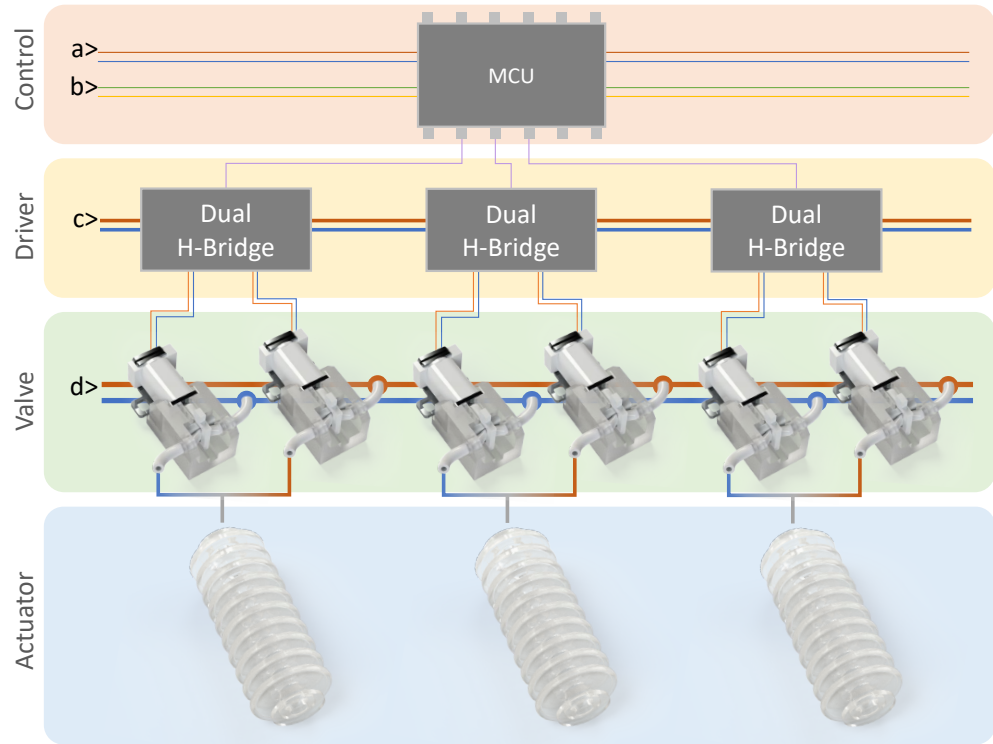


Figure 4.3: Schematic structure of the control circuit, EPVs and actuators. a: power supply for the MCU, b: communication bus, c: power supply for solenoids, d: pressure supplies.

The first MCU used for the circuit is STM32F030F4, which has a TSSOP-20 package with 15 GPIOs,

barely enough for communication and control. To get enough IO channels, a 16-bit IO expander (PCA-8575) is added to the circuit, which communicates with the MCU via IIC bus (Figure 4.4). Later the MCU is replaced by STM32F030K6 with 25 GPIOs, so the I/O expander is no longer needed. Both chips have the same ARM core (Cortex-M0) and same clock frequency (8MHz internal clock). An external crystal oscillator can boost the clock speed up to 48MHz if necessary. The voltage required by the MCU is different from the voltage used to drive the solenoid, so the circuit has two different voltage input and a common ground. Communication wires and voltage supplies also go through the wrist in a helix shape and will connect to next module afterwards.

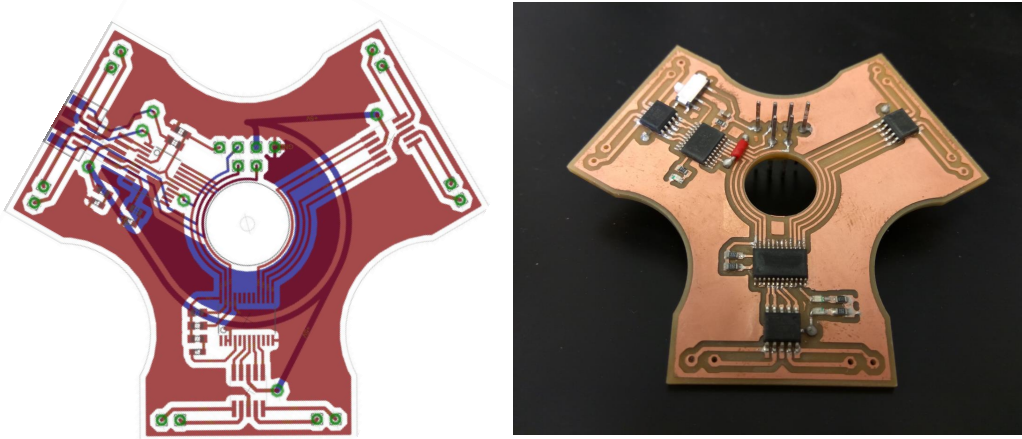


Figure 4.4: Circuit board design and a prototype PCB. The chip on the top left is the MCU, the chip on the bottom is the IO expander. Three dual H-Bridge chips locate on each edge of the PCB.

The circuit boards are made by the Bantam Tools Desktop PCB Milling Machine from double-sided FR-1 PCB blanks. A SMD soldering station is used to solder all the SMD packages. After soldering, the entire circuit is coated by acrylic conformal coating (Techspray 2108) to prevent corruption.

4.1.2 Prototype Wrist

The low profile LTCs and the pressure distributor are merged together and 3D-printed as one part. Then the EMPVs and soft actuators are assembled on it. The complete assembly has a weight of only 110 g. The

radius from the center of the wrist to the outer rim of the actuators is 42.5 mm.

All the parts containing channels are printed with SLA 3D printer. The liquid-based filament will fill up the defects (if there is any) during printing process and will cure with the surrounding into solid afterwards, so the channel is fluid-tight can withstand high pressure. Other supportive parts are printed by Lulzbot Taz 6 using PLA material. The Spine plates are cut from the Delrin acetal resin sheet using the milling machine.

The three hybrid actuators grant three degree of freedom for the wrist. Because the arterial supply and the communication wires do not confine the length of the wrist, this wrist can stretch to any length freely (Figure 4.5 (A) and (B)). Also, it can bend to all the directions (Figure 4.5 (C1) to (C6)).

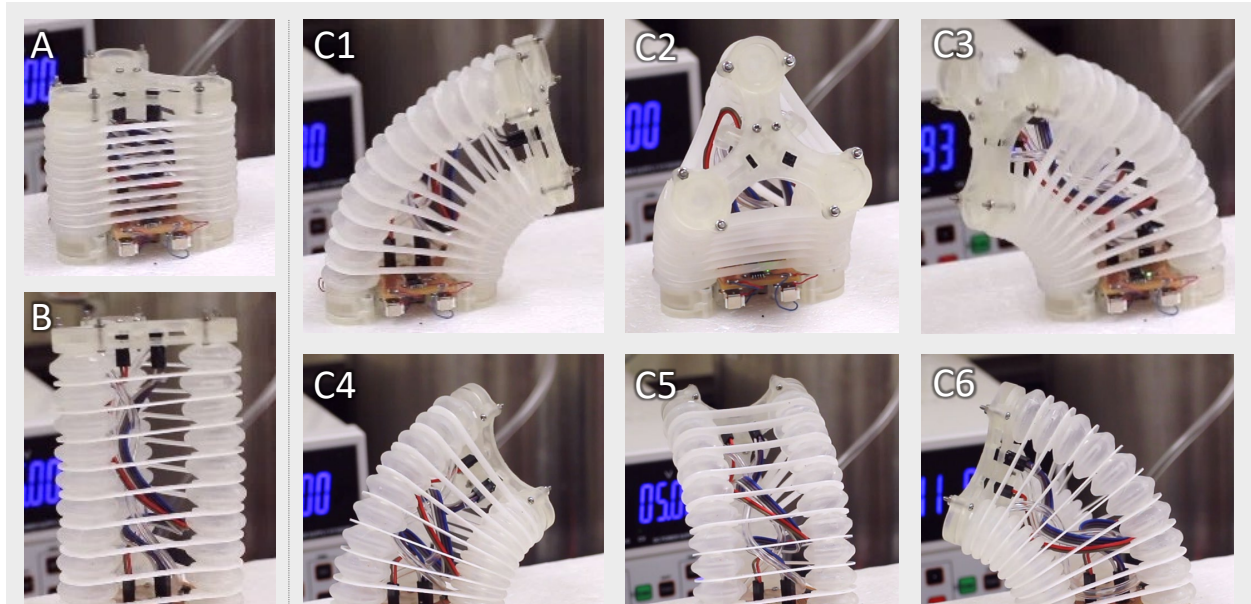


Figure 4.5: A wrist performs fully compressing (A), fully stretching (B), and bending to different directions (C1) to (C6). The circuit design and wire arrangement are slightly different from the one shown above.

4.2 Modular Soft Arm

Now that both pressure supply and communication wires can link in serials, many modules can work together with very simple assembling. By connecting several wrists together, a functional soft arm is made (Figure 4.6). The wrists on an arm receive the command from a central controller and work independently.



Figure 4.6: Rendered soft robotic arm made of three wrists.

Because each wrist has three DoFs, the total DoFs on a long arm are huge and can perform every agile maneuver. Figure 4.7 (A) and (B) show an arm made of two wrists achieving large elongation ratio (200%) between fully contracted and fully stretched state. With two sections being able to freely bend to any directions, they can accomplish more complex posture than a single wrist (Figure 4.7 (C) and (D)).

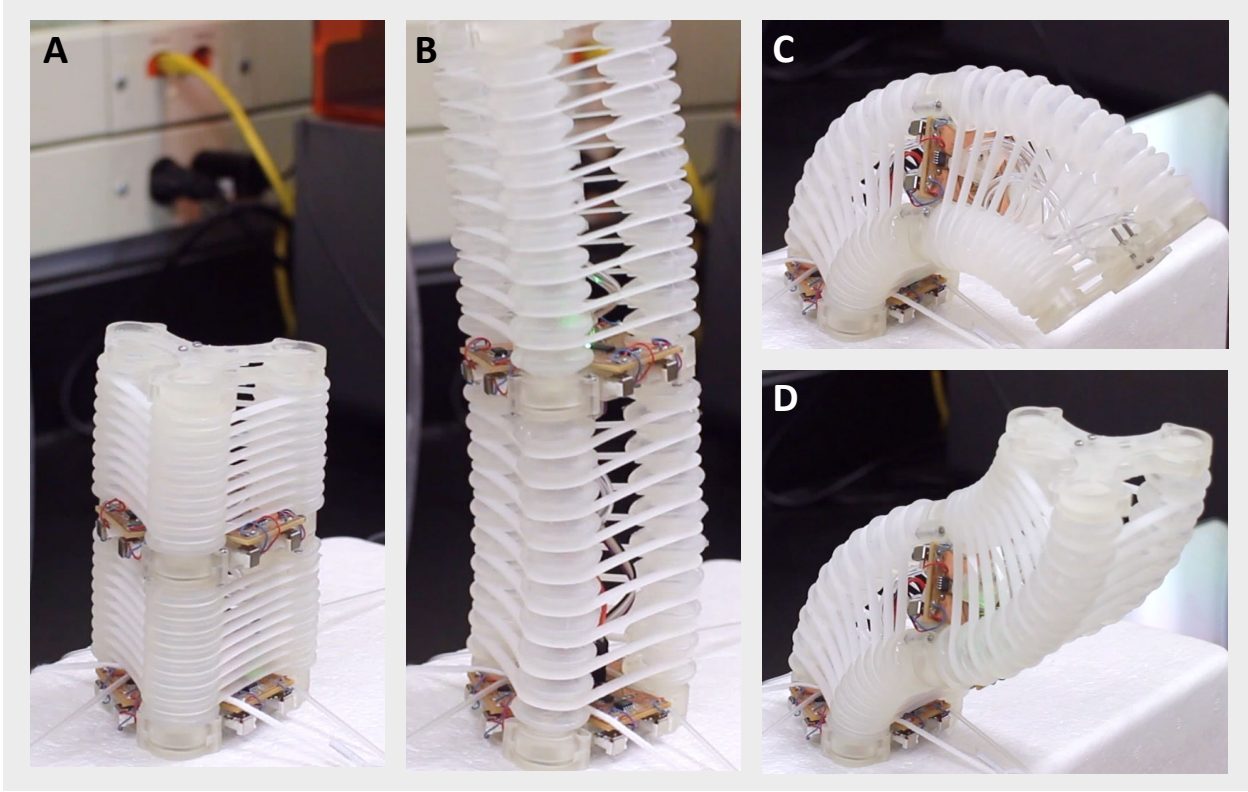


Figure 4.7: An arm with two wrists demonstrates the state of (A) fully contracted, (B) fully stretched, (C) two modules bend towards the same direction, (D) and two modules bend towards opposite directions. Comparing (A) and (B) one can see the length of a fully stretched arm can double its contracted length.

4.3 Isomorphic Synchronous Transmit-Receive

Connecting more sections together makes a functional arm. A three-section arm (Figure 4.8) can reach to a large space while aligning the end-effector to different directions. To effectively control such a modular robot, we also need a communication method that works for identical hardware and software. For most multi-client communication protocols, there will be an address somehow assigned to each node. For example, IIC requires every slave to have a unique address; A USB device does not have a certain address, because the address is assigned to the port on the hub. Either protocol can only support limited number of devices connecting to

the master, because the length for addressing is fixed.

IIC is good for communicating with a series of devices linked end to end, because it uses a common bus to communicate to all the devices, however the master cannot tell the physical locations of the devices. Each device has to be programmed with a unique address by either hardware or software, thus does not allow identical module to be linked together.

In comparison, the root controller of USB can know the physical location of all the devices. USB follows a tree topology; each device communicates with the hub via the port it plugged in. In this way, the master can tell where a device is according to the hub structure. However, the maximum allowed hubs linked in serial is five, thus is not suitable for long modular robots.

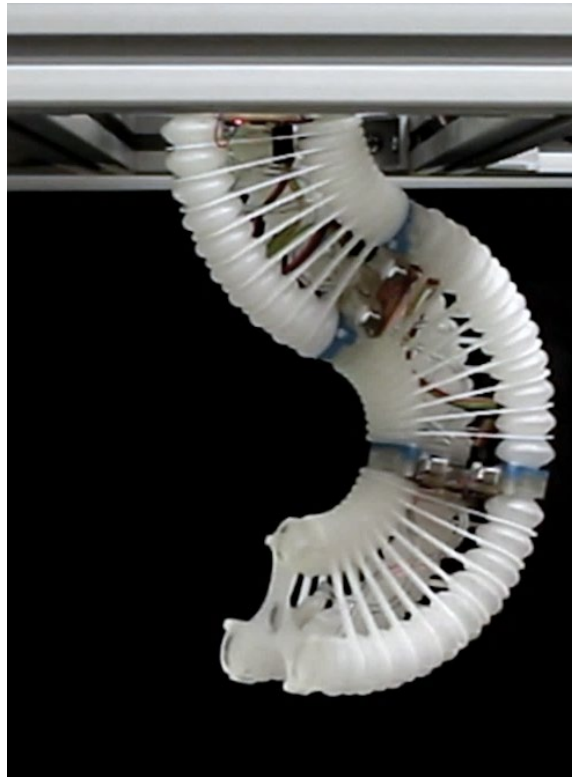


Figure 4.8: A three-section arm controlled by ISTR protocol.

In order to make the modular robot truly “plug and play”, the communication should get rid of both hardware and software address, and a module should act to the command according to its physical location. Here we designed a unique communication method to control the modular arm, which takes the advantage of both protocols: it is simple and easy to implement like IIC, using two wires (or three wires for full-duplex) to communicate to all the devices; meanwhile it delivers data to each module of the robot according to the

topology of the modular structure, requires no specified address for the modules. This is the Isomorphic Synchronous Transmit-Receive (ISTR) protocol.

ISTR is built upon USART, which is commonly supported by MCUs as a specialized peripheral. It requires only three wires for full-duplex communication or two wires for half-duplex. The series of command is packed by the order of the modules, and when the first module receives the data, it will keep the first segment of the data and send the rest to the next module and the next module will repeat the same; When the modules report feedback to the master, every module will report the data it receives from the next module and append its own at the end (Figure 4.9).

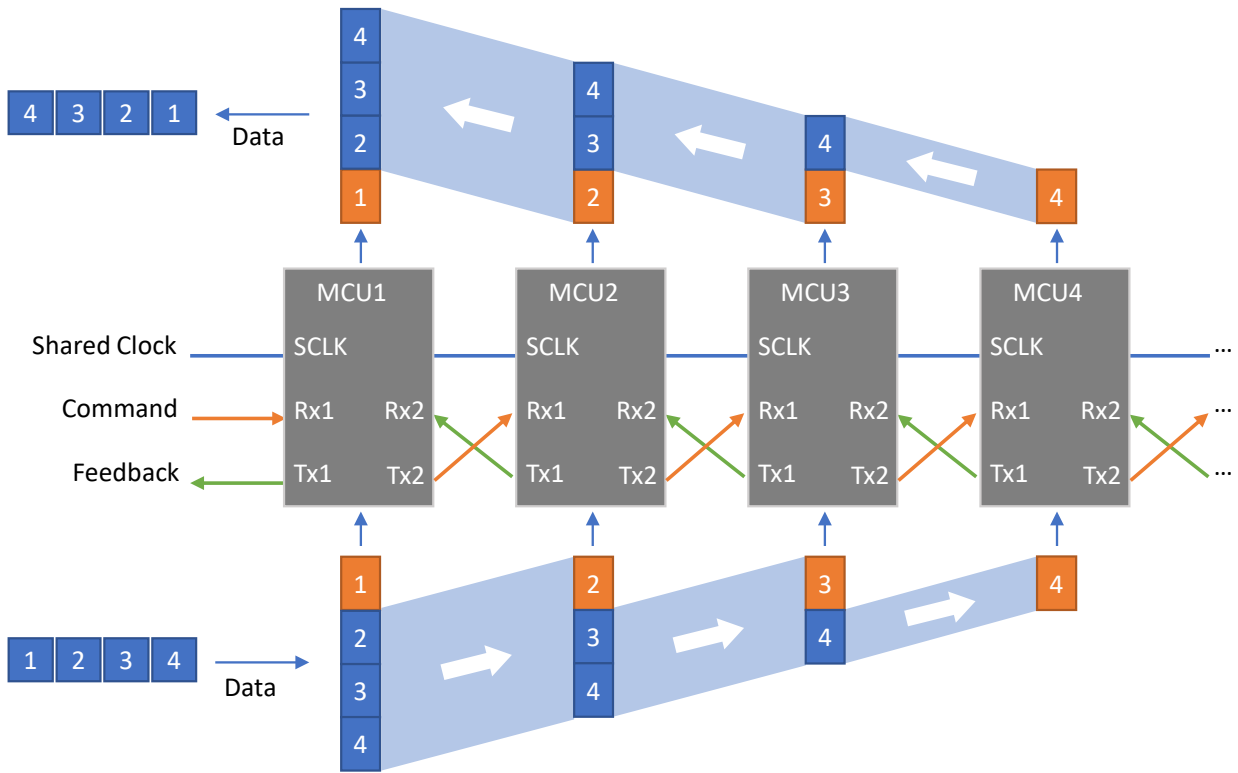


Figure 4.9: The sequence of data sending to and collecting from the modules.

The communication is synchronous, allowing fast and robust transmission with less MCU performance requirement (50kpbs on 8MHz MCU in the prototype). It also allows two special flags: falling-edge and rising-edge on the data wire during HIGH state of SCLK. The timing diagram of ISRT is shown in Figure 4.10, a transmission starts with a falling edge (START flag) and the data for different module is separated by a rising-edge (BRACE flag). Data bits are set during SCLK is LOW and are read during SCLK is HIGH. Two BRACE flags in a row marks the end of the transmission (STOP). During forward transmission, a

module starts to repeat data to the next as soon as the first BRACE is received; and during backward transmission, a module starts to repeat data to the previous as soon as START is received and starts to append its own data after STOP (Figure 4.11). This minimize the communication latency when there are many modules linked together.

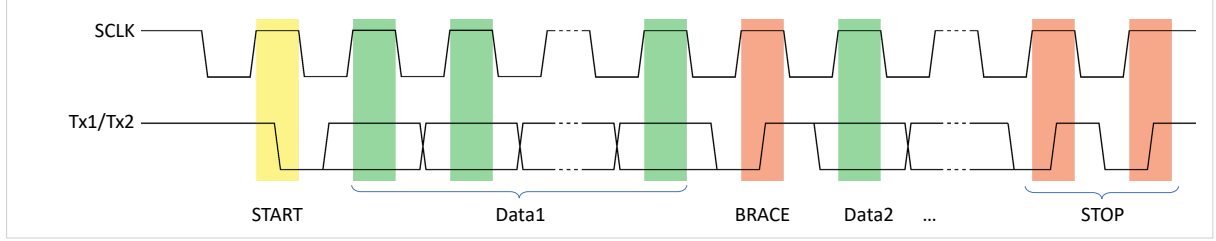


Figure 4.10: Timing Diagrams of ISTR protocol.

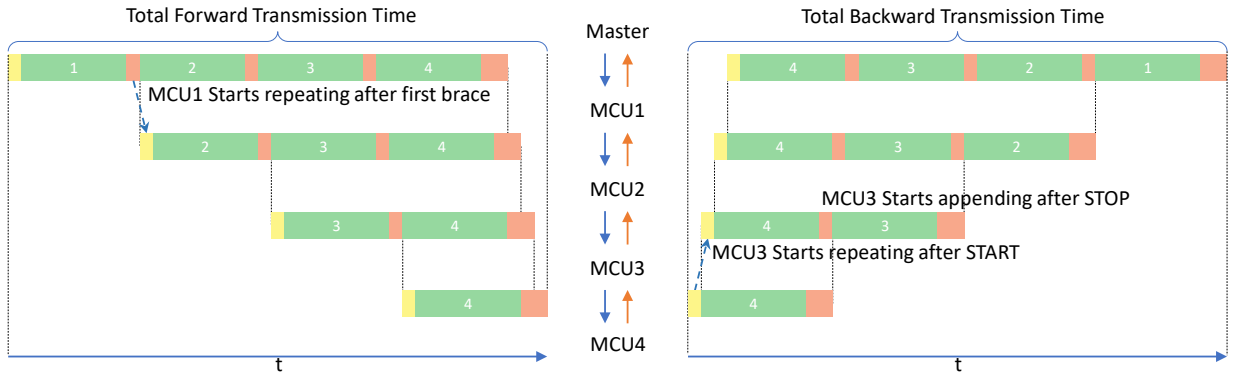


Figure 4.11: Sequence of sending and receiving data of all sections on a four-section arm. One MCU starts repeating/appending data immediately after finishing its own part, minimize the delay as a relay, thus reduce the latency of modules near the end effector on a long arm.

The ISTR runs in half-duplex mode in the prototype multi-wrist arm (single data wire). The only feedback data from the arm are the initial self-checking report, for most of the time data go from the master to the wrists. The communication speed is set to be 50 kHz on the arm, while the maximum tested speed is 400 kHz under 48 MHz clock speed. The maximum communication speed decreases with the increase of communication distance.

Chapter 5

Discussion

Previously, soft robots carrying control components either have very few degrees of freedom or have to be made in large size due to the limitation of traditional valves. With EMPV, one can embed controllers locally onto the soft robots with reasonable additional weight and size. This will boost the density of degrees of freedom on a soft robot, which opens up many new possibilities.

One of the most important applications of the EMPV is to develop highly modularized soft robot. It is not scalable if adding a degree of freedom results in adding a tube that go through the robot. Using EMPV based hybrid actuators, a soft robot only needs constant number of tubes that act as arterial pressure supplies. Each module connects to the arterial individually by the easiest approach. The behavior of every module is controlled locally according to the commands sent from a central controller. In this way, the soft robot acquires the structure of our blood vessels system and nervous system, and such bionic framework even enables more biological inspirations to be implanted into a robot.

The EMPV also has the potential to be made into even smaller size using customized solenoid. So far, the easiest way to convert electric energy to macroscopic motion is still using solenoid. There is no other approach currently available to generate the force and displacement the EMPV requires with reasonable voltage and current.

The soft tube used in the EMPV determines almost all its characteristic. For common off-the-shelf tubes, softer material results in faster closing response and higher shutoff efficiency, but the pressure rating is lower, and it is easier to collapse under negative pressure. With better materials, the performance of EMPV can improve a lot. Fiber-enhanced silicone tubes have thinner wall thickness and more strength while it is easier to be squeezed (smaller F_e), ideal for operating positive pressure. Tubes with thicker wall can improve the opening response time under negative pressure. The tube we used in the prototype is good for universal low-pressure applications.

The hybrid actuator is the basic component for a pneumatic powered modular soft robot. With better manufacturing process and smaller EMPV, the dead length of the hybrid actuator can be further decreased. The soft actuator used in the prototype is hard to mass product in the lab, since the injection process is

complicated and require careful operation to avoid defects. Also, it has to cure under room temperature for a day due to the use of the wax mold. This is the major reason why we did not make a very long arm. The wax residual on the silicone surface also deteriorates the self-sealing ability, results in additional O-rings in the assembly. Using 3D-printed water-soluble PVA inner mold may solve all these problems, but the material is more expensive and not recyclable. However, none of these are concerns if the actuators are produced commercially.

The prototype modular wrist is a primitive design using hybrid actuators. The circuit board and the solenoid valves are exposed outside the module for easy access and debugging. Now that the module has been fully tested, a new design will put everything within the outline of the three actuators.

Another problem for the modular robot is the power supply. If many modules are linked in series, the voltage drop along the robot is not neglectable, especially when the current consumption is high. This can be solved by adding a buck converter to every module and use higher supply voltage. The buck converter steps down voltage while stepping up current from its input (supply) to its output (load), thus the supply current can decrease, reducing the ohmic loss along the wires and contacts.

The ISTR protocol is not directly supported by a hardware peripheral on the MCU because the customized flags used in the communication. This results in additional loads for the ARM core. Besides, the lack of buffer and error check will be a problem for large scale applications, though in the prototype arm the communication works soundly. We have not adapted the protocol for robots with branches, currently it only works for linear robots. Since the bit rate on the main data wire is constant, the communication speed will decrease after a branch structure (which is the case for any communication with tree topology).

The EMPV had a tedious name when it was proposed – “Vasoconstriction-like fluid regulator”. The aim was to mimic how we control the blood flow in our organs. This work is still far away from imitating this biogenic process, however it shows a way to amplify a tiny force and control a soft robot. This structure can also be used in the future if micro actuators better than solenoids are developed.

References

- [1] Jamshed Iqbal, Ahmad Tahir, Muhammad Ul Islam, and Riaz-un-Nabi . Robotics for nuclear power plants — challenges and future perspectives. pages 151–156, 09 2012.
- [2] Floyd E. Gelhaus and Harry T. Roman. Robot applications in nuclear power plants. *Progress in Nuclear Energy*, 23(1):1 – 33, 1990.
- [3] Sangbae Kim, Cecilia Laschi, and Barry Trimmer. Soft robotics: A bioinspired evolution in robotics. *Trends in Biotechnology*, 31(5):287–294, 2013.
- [4] Deepak Trivedi, Christopher D. Rahn, William M. Kier, and Ian D. Walker. Soft robotics: Biological inspiration, state of the art, and future research. *Applied Bionics and Biomechanics*, 5(3):99–117, 2008.
- [5] Daniela Rus and Michael T. Tolley. Design, fabrication and control of soft robots. *Nature*, 521(7553):467–475, 2015.
- [6] Kyu Jin Cho, Je Sung Koh, Sangwoo Kim, Won Shik Chu, Yongtaek Hong, and Sung Hoon Ahn. Review of manufacturing processes for soft biomimetic robots. *International Journal of Precision Engineering and Manufacturing*, 10(3):171–181, 2009.
- [7] E T L Project. Experiences of Teaching & Learning Questionnaire. *ETL Project Enhancing Teaching-Learning Environments in Undergraduate Courses*, pages 5289–5296, 2002.
- [8] Joseph T. Muth, Daniel M. Vogt, Ryan L. Truby, Yi it Mengüç, David B. Kolesky, Robert J. Wood, and Jennifer A. Lewis. Embedded 3D printing of strain sensors within highly stretchable elastomers. *Advanced Materials*, 26(36):6307–6312, 2014.
- [9] Asli Atalay, Vanessa Sanchez, Ozgur Atalay, Daniel M. Vogt, Florian Haufe, Robert J. Wood, and Conor J. Walsh. Batch Fabrication of Customizable Silicone-Textile Composite Capacitive Strain Sensors for Human Motion Tracking. *Advanced Materials Technologies*, 2(9):1–8, 2017.
- [10] Charles M. Best, Morgan T. Gillespie, Phillip Hyatt, Levi Rupert, Vallan Sherrod, and Marc D. Killpack. A New Soft Robot Control Method: Using Model Predictive Control for a Pneumatically Actuated Humanoid. *IEEE Robotics and Automation Magazine*, 23(3):75–84, 2016.
- [11] Cagdas D. Onal and Daniela Rus. Autonomous undulatory serpentine locomotion utilizing body dynamics of a fluidic soft robot. *Bioinspiration and Biomimetics*, 8(2), 2013.
- [12] Bobak Mosadegh, Panagiotis Polygerinos, Christoph Keplinger, Sophia Wennstedt, Robert F. Shepherd, Unmukt Gupta, Jongmin Shim, Katia Bertoldi, Conor J. Walsh, and George M. Whitesides. Pneumatic networks for soft robotics that actuate rapidly. *Advanced Functional Materials*, 24(15):2163–2170, 2014.
- [13] Kevin C Galloway, Panagiotis Polygerinos, Conor J Walsh, and Robert J Wood. Mechanically Programmable Bend Radius for Fiber-Reinforced Soft Actuators. 2013.
- [14] Fionnuala Connolly, Panagiotis Polygerinos, Conor J. Walsh, and Katia Bertoldi. Mechanical Programming of Soft Actuators by Varying Fiber Angle. *Soft Robotics*, 2(1):26–32, 2015.

- [15] Panagiotis Polygerinos, Zheng Wang, Johannes T B Overvelde, Kevin C. Galloway, Robert J. Wood, Katia Bertoldi, and Conor J. Walsh. Modeling of Soft Fiber-Reinforced Bending Actuators. *IEEE Transactions on Robotics*, 31(3):778–789, 2015.
- [16] Soo Jin Adrian Koh, Xuanhe Zhao, and Zhigang Suo. Maximal energy that can be converted by a dielectric elastomer generator. *Applied Physics Letters*, 94(26), 2009.
- [17] Ron Pelrine, Roy Kornbluh, Qibing Pei, and Jose Joseph. High-speed electrically actuated elastomers with strain greater than 100%. *Science*, 287:836–839, 2000.
- [18] M Shahinpoor, Y Bar-Cohen, J O Simpson, and J Smith. Ionic polymer-metal composites (ipmcs) as biomimetic sensors, actuators and artificial muscles - a review. *Smart Materials and Structures*, 7(6):R15, 1998.
- [19] R.A. Russell and R.B. Gorbet. Improving the response of SMA actuators. *Proceedings of 1995 IEEE International Conference on Robotics and Automation*, 3:2299–2304, 2000.
- [20] Paxton Maeder-York, Tyler Clites, Emily Boggs, Ryan Neff, Panagiotis Polygerinos, Dónal Holland, Leia Stirling, Kevin Galloway, Catherine Wee, and Conor Walsh. Biologically Inspired Soft Robot for Thumb Rehabilitation. Technical report.
- [21] Panagiotis Polygerinos, Stacey Lyne, Zheng Wang, Luis Fernando Nicolini, Bobak Mosadegh, George M Whitesides, and Conor J Walsh. Towards a soft pneumatic glove for hand rehabilitation. In *Intelligent Robots and Systems (IROS), 2013 IEEE/RSJ International Conference on*, page 1512{‐}1517, 2013.
- [22] *Soft Pneumatic Artificial Muscles With Low Threshold Pressures for a Cardiac Compression Device*, volume 6A, Portland, OR, 2013. ASME.
- [23] Andrew D. Marchese, Robert K. Katzschmann, and Daniela Rus. A recipe for soft fluidic elastomer robots. *Soft Robotics*, 2(1):7–25, 2015. PMID: 27625913.
- [24] Alex Nemiroski, Yanina Y. Shevchenko, Adam A. Stokes, Baris Unal, Alar Ainla, Sahradha Albert, Gabrielle Compton, Emily MacDonald, Yosyp Schwab, Caroline Zellhofer, and George M. Whitesides. Arthrobots. *Soft Robotics*, 4(3):soro.2016.0043, 2017.
- [25] Hao Jiang, Xinghua Liu, Xiaotong Chen, Zhanchi Wang, Yusong Jin, and Xiaoping Chen. Design and simulation analysis of a soft manipulator based on honeycomb pneumatic networks. *2016 IEEE International Conference on Robotics and Biomimetics, ROBIO 2016*, pages 350–356, 2017.
- [26] Robert K. Katzschmann, Andrew D. Marchese, and Daniela Rus. Autonomous Object Manipulation Using a Soft Planar Grasping Manipulator. *Soft Robotics*, 2(4):155–164, 2015.
- [27] Andrew D. Marchese, Robert K. Katzschmann, and Daniela Rus. Whole arm planning for a soft and highly compliant 2D robotic manipulator. In *2014 IEEE/RSJ International Conference on Intelligent Robots and Systems*, pages 554–560. IEEE, sep 2014.
- [28] Michael T. Tolley, Robert F. Shepherd, Bobak Mosadegh, Kevin C. Galloway, Michael Wehner, Michael Karpelson, Robert J. Wood, and George M. Whitesides. A Resilient, Untethered Soft Robot. *Soft Robotics*, 1(3):213–223, 2014.
- [29] R. Cohen, M. G. Lipton, M. Q. Dai, and B. Benhabib. Conceptual Design of a Modular Robot. *Journal of Mechanical Design*, 114(1):117, 1992.
- [30] A. Kamimura, S. Murata, E. Yoshida, H. Kurokawa, K. Tomita, and S. Kokaji. Self-reconfigurable modular robot - experiments on reconfiguration and locomotion. In *Proceedings 2001 IEEE/RSJ International Conference on Intelligent Robots and Systems. Expanding the Societal Role of Robotics in the the Next Millennium (Cat. No.01CH37180)*, volume 1, pages 606–612 vol.1, Oct 2001.

- [31] Yuchao Zhang, Hongxing Wei, Bo Yang, and Cancan Jiang. Sambot II: A self-assembly modular swarm robot. *AIP Conference Proceedings*, 1955(37), 2018.
- [32] Matthew A. Robertson and Jamie Paik. New soft robots really suck: Vacuum-powered systems empower diverse capabilities. *Science Robotics*, 2(9), 2017.
- [33] Alex Zatopa, Steph Walker, and Yigit Menguc. Fully Soft 3D-Printed Electroactive Fluidic Valve for Soft Hydraulic Robots. *Soft Robotics*, 5(3):soro.2017.0019, 2018.